Clim Dyn (2015) 45:2213–2235
DOI 10.1007/s00382-015-2469-5

Decadal predictability of soil water, vegetation, and wildfire frequency over North America

Yoshimitsu Chikamoto · Axel Timmermann · Samantha Stevenson · Pedro DiNezio · Sally Langford

Received: 27 May 2014 / Accepted: 4 January 2015 / Published online: 18 January 2015
© The Author(s) 2015. This article is published with open access at Springerlink.com

Abstract The potential decadal predictability of land hydrological and biogeochemical variables in North America is examined using a 900-year-long pre-industrial control simulation, conducted with the NCAR Community Earth System Model (CESM) version 1.0.3. The leading modes of simulated North American precipitation and soil water storage are characterized essentially by qualitatively similar meridional seesaw patterns associated with the activity of the westerly jet. Whereas the corresponding precipitation variability can be described as a white noise stochastic process, power spectra of vertically integrated soil water exhibit significant redness on timescales of years to decades, since the predictability of soil water storage arises mostly from the integration of precipitation variability. As a result, damped persistence hindcasts following a 1st order Markov process are skillful with lead times of up to several years. This potential multi-year skill estimate is consistent with ensemble hindcasts conducted with the CESM for various initial conditions. Our control simulation further suggests that decadal variations in soil water storage also affect vegetation and wildfire occurrences. The long-term potential predictability of soil water variations in combination with the slow regrowth of vegetation after major disruptions leads to enhanced predictability on decadal timescales for vegetation, terrestrial carbon stock, and fire frequency, in particular in the Southern United States (US)/Mexico region. By contrast, the prediction skill of fire frequency in the Northern US is limited to 1 year. Our results demonstrate that skillful decadal predictions of soil water storage, carbon stock, and fire frequency are feasible with proper initialization of soil conditions. Although the potential predictability in our idealized modeling framework would overestimate the real predictability of the coupled climate-land-vegetation system, the decadal climate prediction may become beneficial for water resource management, forestry, and agriculture.

Keywords Decadal climate prediction · Land hydrological process · Earth system model

Y. Chikamoto (✉) · A. Timmermann · P. DiNezio
IPRC, University of Hawaii at Manoa, 1680 East-West Road, Honolulu, HI 96822, USA
e-mail: chika44@hawaii.edu

S. Stevenson
Climate and Global Dynamics Division, National Center for Atmospheric Research, Boulder, CO, USA

S. Langford
Department of Atmospheric and Oceanic Sciences, CIRES, University of Colorado Boulder, Boulder, CO, USA

1 Introduction

Below-normal water storage in soils and aquifers impacts agriculture, forest fires, and water management. This is especially important for arid regions, such as some portions of North America (Svoboda et al. 2002; Dai 2011). A prominent example of massive soil drying was the "Dust Bowl" in the 1930s (Woodhouse and Overpeck 1998), which caused massive crop failures and other large-scale socio-economic impacts (Schubert et al. 2004; Cook et al. 2009). Furthermore, dry soil conditions may lead to an increased probability of wildfires (Thonicke et al. 2001; Thornley and Cannell 2004), impacting human livelihoods, ecosystems, the carbon cycle, and air quality (Kloster et al. 2010). In view of the potential societal threats, drought conditions in the United States (US) are carefully monitored and considerable efforts are made to forecast hydroclimate conditions on seasonal timescales (Svoboda et al. 2002; Schubert et al. 2007).

Whereas precipitation itself has low predictive skill beyond one season (Collins 2002; Alessandri et al. 2011), the soil moisture content is generally predictable for several seasons ahead due to the high persistence associated with the weak damping effect of soil hydrological processes (Delworth and Manabe 1988; Wu et al. 2002; Arora and Boer 2006). Seasonal predictions of soil moisture content over the US, in turn, have been shown to improve predictability of precipitation and temperature variations (Wang and Kumar 1998; Kanamitsu et al. 2003). The enhanced predictability originates from the fact that soils can integrate precipitation and evaporation noise (Delworth and Manabe 1988; Wu et al. 2002; Arora and Boer 2006). As a result of soil and atmosphere feedbacks (Beljaars et al. 1996; Seneviratne et al. 2010), seasonal predictions of soil moisture content over the US can further increase the predictability of precipitation and atmospheric temperature variations for up to several months (Zeng et al. 1999; Kanamitsu et al. 2003; Koster and Suarez 2003; Yang et al. 2004; Dirmeyer et al. 2013).

Although anthropogenic climate change over the next century is likely to reduce soil moisture content in large areas of the southern continental US (Shin and Sardeshmukh 2011; Dai 2013), the real climate trajectory in the coming decades will be influenced by a combination of external radiative boundary conditions and internally occurring climate variability (Smith et al. 2007; Keenlyside et al. 2008; Mochizuki et al. 2010; van Oldenborgh et al. 2012; Chikamoto et al. 2013; Meehl et al. 2013). Therefore, decadal hydrological prediction requires an understanding of both the externally forced component and the prediction skill of internally generated decadal hydroclimate variability. However, the predictive skill of real climate predictions is contaminated by model deficiencies and observational uncertainties (Meehl et al. 2014). Model experiments should be the most appropriate way to estimate the predictive skill of internal variability in the absence of these real-world effects.

Our study addresses the basic research question of whether the soil water condition and wildfire occurrence are predictable *on timescales beyond several years*. Using a *perfect* modeling framework, we set out to determine the upper limits of predictability for precipitation, soil moisture and forest fire risk in the US.

This paper is organized in two parts. The first part of the paper (Sects. 2, 3) introduces the numerical model experiments conducted with the NCAR Community Earth System Model (CESM) version 1.0.3 and a simple concept of soil water storage based on a stochastic process. The main concept is that soils are long-term integrators of the net water balance composed of precipitation, evaporanspiration, and runoff. This integration of white noise variability (Hasselmann 1976) leads to enhanced soil water variability at lower frequencies and potential longer-term predictability (Delworth and Manabe 1988). Applying the framework of Delworth and Manabe (1988) to the more complex CESM system, we compare simple red noise null hypothesis models for soil moisture variations at various depth levels with an ensemble of perfect model forecasts conducted with the CESM. The second part of our study (Sect. 4) focuses on the effects of soil moisture variations on North American vegetation and wildfire occurrences. The CESM ensemble predictions are then used to determine potential multi-year skill of simulated variations in North American wildfire frequency and terrestrial carbon stocks. We discuss the limitations of our idealized modeling framework in Sect. 5, and conclude this study in Sect. 6.

2 Model experiment

2.1 Model set up and prediction experiments

In this study, we use the fully coupled low resolution earth system model CESM 1.0.3 (Shields et al. 2012). The model physics is largely based on the Community Climate System Model version 4 (Gent et al. 2011), which includes atmospheric physics of the Community Atmosphere Model version 4 (CAM4) (Neale et al. 2013). The atmospheric and land resolutions are T31 spectral (approximately 3.75° resolution) with hybrid sigma pressure coordinate of 26 atmospheric levels from sea level to 1 hPa and 15 soil levels from surface to the bottom layer of 35 m. The 60 level ocean model is coupled with the sea-ice component and uses a horizontal resolution of approximately 3° with a displaced North Pole. The atmosphere, land, and sea ice components communicate every 30 min whereas the ocean component is coupled with atmosphere once a day. From these components, we can obtain monthly outputs. The land component is the Community Land Model version 4 (CLM4), which includes a carbon–nitrogen biogeochemical cycle, a simple groundwater model, and a wildfire scheme (Lawrence et al. 2012). Total water storage in CLM4 is represented by soil moisture content in 2.9 m total depth with 10 soil layers and aquifer water with changing water table depth. Soil moisture in the bottom layer interacts with aquifer water below through a diffusion process. These schemes improve the representation of observed land hydrological processes such as runoff, evapotranspiration, and soil water storage (Niu and Yang 2007; Oleson et al. 2008). In the fire scheme of CLM4, wildfire occurrence in each grid box is parameterized in terms of fuel density obtained from the vegetation carbon, hydrological conditions, and temperature (Thonicke et al. 2001; Kloster et al. 2010). Details of the model basic performance in the low resolution version can be found in Shields et al. (2012).

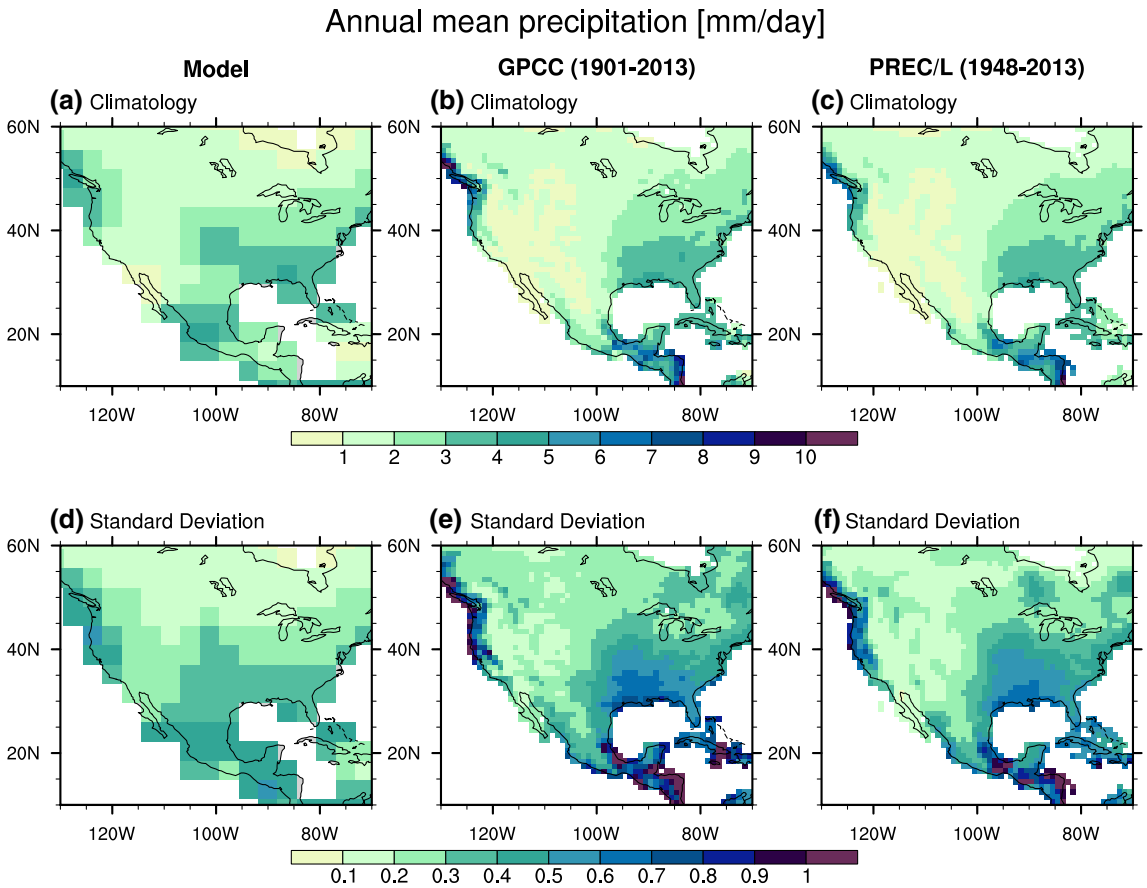

Fig. 1 Climatology (*top*) and standard deviation (*bottom*) of annual mean precipitation in Model CTL run for 900-years (*left*), GPCC for the 1901–2013 period (*center*), and PREC/L for the 1948–2013 period (*right panels*)

Following a 100-year coupled model spin-up, we perform a 900-year-long pre-industrial control simulation (CTL run) using constant greenhouse gas conditions for the year 1850 CE. This long simulation enables us to identify the leading patterns of decadal-to-multidecadal hydroclimate variability over North America. We use this CTL run as a surrogate "real" world and then evaluate the predictability by hindcasting this model simulated climate variability. This approach allows us to neglect observational errors and model biases, and is therefore referred to as the *perfect* modeling framework. Using a total of 39 initial conditions chosen every five years on January 1st, we conduct 10-year-long ensemble hindcast experiments. This hindcast setting roughly follows the experimental design of the Coupled Model Intercomparison Project-5 (CMIP5) for decadal climate prediction (Taylor et al. 2009; Murphy et al. 2010). For the ensemble generation, we add small random perturbations into atmospheric prognostic variables but keep the same initial conditions of ocean and land in the CTL run. The ensemble of atmospheric initial conditions is generated by rescaling the difference between current Y_i and previous Y_{i-n} initial conditions in the pre-industrial control simulation with a factor of $\pm 1\,\%$ (i.e., $Y_i' = Y_i + \alpha(Y_i - Y_{i-n})$, where Y_i and Y_i' are the control and perturbed initial conditions, $\alpha = \pm 0.01$ and $n = 1, 2, 3, 4,$ and 5 years). This approach allows us to estimate the maximum predictability of the decadal anomalies assuming perfect knowledge of the initial state of the ocean and land.

2.2 Model validation

The large-scale distributions of climatological precipitation simulated by the CTL run of the low resolution CESM 1.0.3 are in good agreement with observations over North America. Figure 1 shows the climatology and standard deviation for annual mean precipitation in the CTL run and observations. We use the 1° observational precipitation datasets from Global Precipitation Climatology Centre (GPCC) version 6 for the 1901–2013 period (Schneider et al. 2011) and Precipitation Reconstruction over Land (PREC/L) for the 1948–2013 period (Chen et al. 2002). Compared to the observations, the simulated annual mean precipitation is reduced in the coastal area surrounding the Gulf of Mexico, the east coast of the US, and the west coast

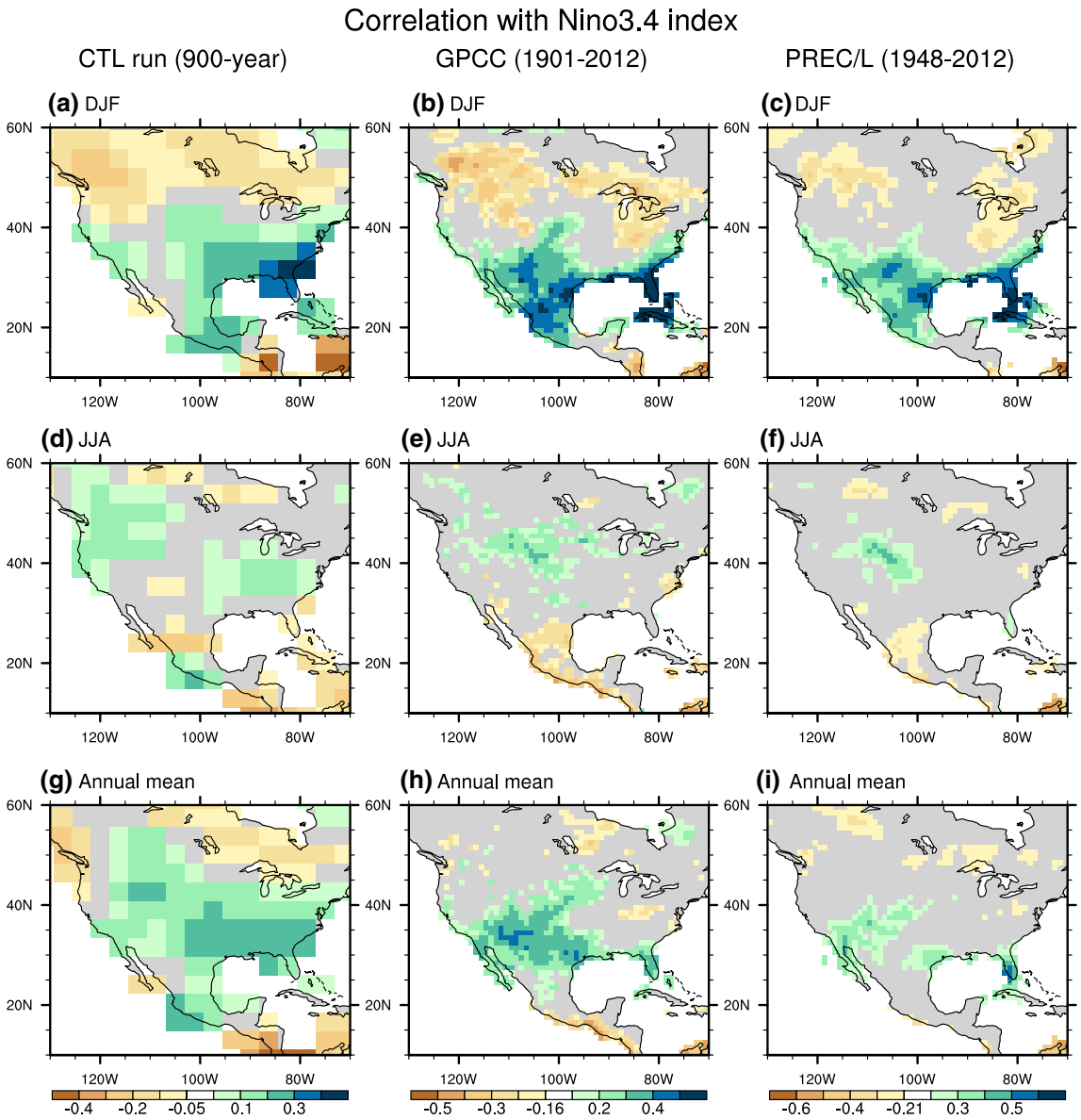

Fig. 2 Correlation maps of DJF (*top*), JJA (*middle*), and annual mean precipitations (*bottom*) with Niño 3.4 index. *Left*, *center*, and *right panels* are the CTL run for 900 years, GPCC for the 1901–2012 period, and PREC/L for the 1948–2012 period. Niño 3.4 index is obtained from SST anomalies (5°S–5°N, 170°W–120°W) in the CTL run or ERSST for the 1850–2012 period. Correlation coefficients of 0.05, 0.16 and 0.21 correspond to the statistical significant at 90 % level with 900, 110, and 60 degrees of freedom in two-side Student *t* test

in the higher latitude region of North America (> 40°N) and enhanced in the Rocky Mountain area (Fig. 1a–c). Due to the fact that rainfall is approximately gamma-distributed, annual mean biases also correspond to biases in the standard deviations of annual mean precipitation (Fig. 1d–f). Irrespective to these smaller-scale biases, the observed large-scale climatological rainfall distribution is reasonably well captured by the CTL run.

In addition to the realistic simulation of climatological precipitation, the CTL run shows reasonable performance for the remote impact of the El Niño Southern Oscillation (ENSO) on precipitation variability in North America. Figure 2 shows simultaneous correlation maps of simulated seasonal and annual mean precipitation with the Niño 3.4 index. For comparison with the observations, we use the NOAA Extended Reconstructed SST version 3 (ERSST) dataset for the 1850–2012 period (Smith et al. 2008). During boreal winter, both the model and observation show the meridional seesaw of precipitation anomalies straddling 40°N associated with the mature phase of El Niño (top panels in Fig. 2). In other words, the CTL run can represent the ENSO teleconnection very well

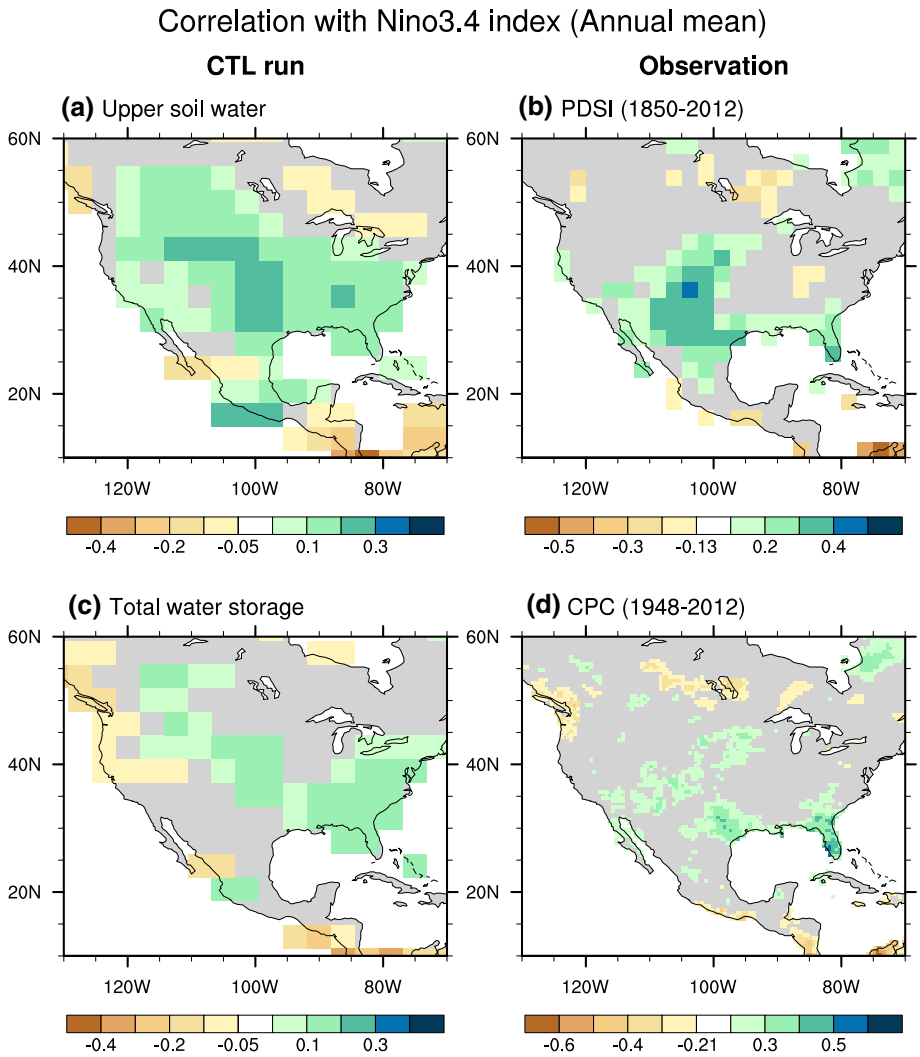

Fig. 3 Same as the bottom panels in Fig. 2 but for **a** soil water within the upper 10 cm levels in the CTL run, **b** the observed PDSI for the 1850–2012 period, **c** total water storage in the CTL run, and **d** soil water in CPC for the 1948–2012 period. Correlation coefficients of 0.05, 0.13, and 0.21 correspond to the statistical significant at 90 % level with 900, 160, and 60 degrees of freedom in two-side Student *t* test, respectively

as pointed out by other studies using the low resolution CESM (Jochum et al. 2009; Stevenson et al. 2012, 2014). During boreal summer, on the other hand, the center of positive correlation is weaker and shifts northward, thus counteracting the effect of negative winter precipitation anomalies in some areas. This seasonality of ENSO teleconnections is consistent with the model experiments by Wang et al. (2013). As as result of the seasonal cancellation of ENSO-induced rainfall anomalies, the annual mean correlation tends to be weaker than the winter values (bottom panels in Fig. 2).

Comparing the simulated upper soil water response to ENSO over North America with the observed one taken from the monthly self-calibrated Palmer Drought Severity Index (PDSI) for the 1850–2012 period (Dai 2011, 2013), we find a good qualitative agreement (Fig. 3a, b). On the other hand, the agreement between ENSO's effect on total soil water in the CTL simulation and the respective diagnostic in the monthly soil water data from the Climate Prediction Center (CPC) for the 1948–2012 period (van den Dool et al. 2003) is considerably weaker compared to those on precipitation and upper soil water. Only the Pacific Northwest, Florida, and Texas show consistent response to ENSO in both model and reanalysis data with local correlations attaining values of only 0.2–0.4. The relatively weak relationship between deep soil water content and ENSO has also been reported in previous studies (Chen and Kumar 2002, 2004). This implies that other modes of climate variability, rather than ENSO, are essential in driving the bulk of soil water variability of North America.

Overall, we find that the CTL simulation in the low resolution CESM captures the larger-scale patterns of seasonal rainfall and its variability associated with ENSO reasonably well. This suggests that the main conclusions from our study on the long-term predictability of hydrological processes are likely to hold for the higher resolution models and the real world.

3 Dynamics and predictability of precipitation and soil water storage

3.1 Analysis of pre-industrial control simulation

To identify the predictable components of land hydrological processes in CESM over North America, we first examine the relationship between precipitation and total water storage via Empirical Orthogonal Function (EOF) analysis. By applying the EOF analysis to individual fields, we can isolate the different timescales of variability. Total water storage here includes the depth-integrated soil moisture content of the soil layer, as well as water stored in aquifers. Although the total amount of water storage is largely determined by the water amount in aquifers, temporal variability of total water storage highly correlates with the total water content variability integrated in the whole soil layers without aquifer water because of the interaction between water in the bottom soil layer and the aquifer. Figure 4 shows the first EOF modes of annual mean precipitation (Fig. 4a) and total water storage (Fig. 4g). They have similar spatial patterns and display a meridional seesaw with a zero-crossing near 35°N. The pattern is closely related to fluctuations in the westerly jet downstream over North America (upper panels in Fig. 5), as described below. In contrast to the spatial similarity, the temporal variations of these first principal components have very different timescales: annual precipitation variability exhibits uniform variability at all timescales characterized by a white power spectrum (Fig. 4b, c), whereas the spectrum of total water storage exhibits more pronounced variability on decadal to centennial timescales (Fig. 4h, i). The difference in the precipitation and soil water spectra suggests that soils and aquifers integrate the water fluxes associated with random atmospheric variability (Amenu et al. 2005; Katul et al. 2007).

In CESM, temporal variations of total water storage W_T balance source and sink terms associated with precipitation P, snowmelt S, evapotranspiration E, and total runoff R:

$$\frac{dW_T}{dt} = P + S - E - R. \tag{1}$$

Following Delworth and Manabe (1988) and Eq. (1), we can create a simplified conceptual model for temporal variations of total water storage for the CESM, which follows stochastic bucket model dynamics. This model is a specific application of the stochastic climate model concept of Hasselmann (1976). For Eq. (1) we assume that the evapotranspiration E and the total runoff R are linearly proportional to the total water storage. This leads to an equation with a linear damping in W_T, reading

$$\frac{dW_T}{dt} = -\epsilon\, \alpha W_T - f\, W_T + (P + S), \tag{2}$$

where ϵ represents a constant value of potential evaporation, according to Delworth and Manabe (1988), α represents another scaling factor associated with the field type which we consider constant in time, and f is a constant value related to the total runoff. Next we assume that S can be neglected by taking annual mean and P can be approximated as a white noise process. According to these simplifying assumptions, variations of total water storage can be expressed in terms of a first-order Markov process (or autoregressive process) forced by the white noise precipitation variability:

$$\frac{dW_T}{dt} = -\lambda\, W_T(t) + P(t) \tag{3}$$

where λ represents the net damping parameter, which also determines predictability associated with the damped persistence. This equation is equivalent to the following finite-difference form: $W_T(t+1) = (1-\lambda)\, W_T(t) + P^*(t)$. When we assume that $P^*(t)$ is the white noise forcing, we can obtain the parameter $(1-\lambda)$ from the lag-1 autocorrelation coefficient of $W_T(t)$. Note that we use annual mean data in our analysis, so the shortest resolvable period in our spectra is 2 years. Resulting red noise power spectra for soil processes were previously described in Delworth and Manabe (1988) and Katul et al. (2007).

We apply this simplified conceptual model to the principal components of precipitation and total water storage (Fig. 4). Choosing the first principal component for annual precipitation as the forcing $P^*(t)$ and using the lag-1 year autocorrelation coefficient of the principal component of total water storage as $(1-\lambda)$, we find a high correlation between the reconstructed $W_T(t)$ variability from Eq. (3) (solid line in Fig. 4h) and the first principal component of total water storage (red and blue bars in Fig. 4h) of 0.76 (significant above the 99 % level). Although precipitation shows white noise variability, the integration of its variability, in particular its low frequency spectral component, plays a key role in generating decadal-to-multidecadal changes in total water storage across North America.

To further test the relationship between total water storage and low frequency precipitation variability, we apply a 10-year running mean filter to the simulated precipitation over land and perform an EOF analysis of the outcome. The resulting first EOF mode (middle panels in Fig. 4) shows the same meridional seesaw pattern as the leading EOFs of unfiltered annual mean precipitation and water storage. The corresponding 1st principal component is highly correlated with the principal component of total water storage (correlation coefficient is 0.70 at a 5 year lag). This finding is consistent with the idea that soils provide a natural low-pass filter (integrator) for precipitation variability, yielding the low frequency signals in total water storage.

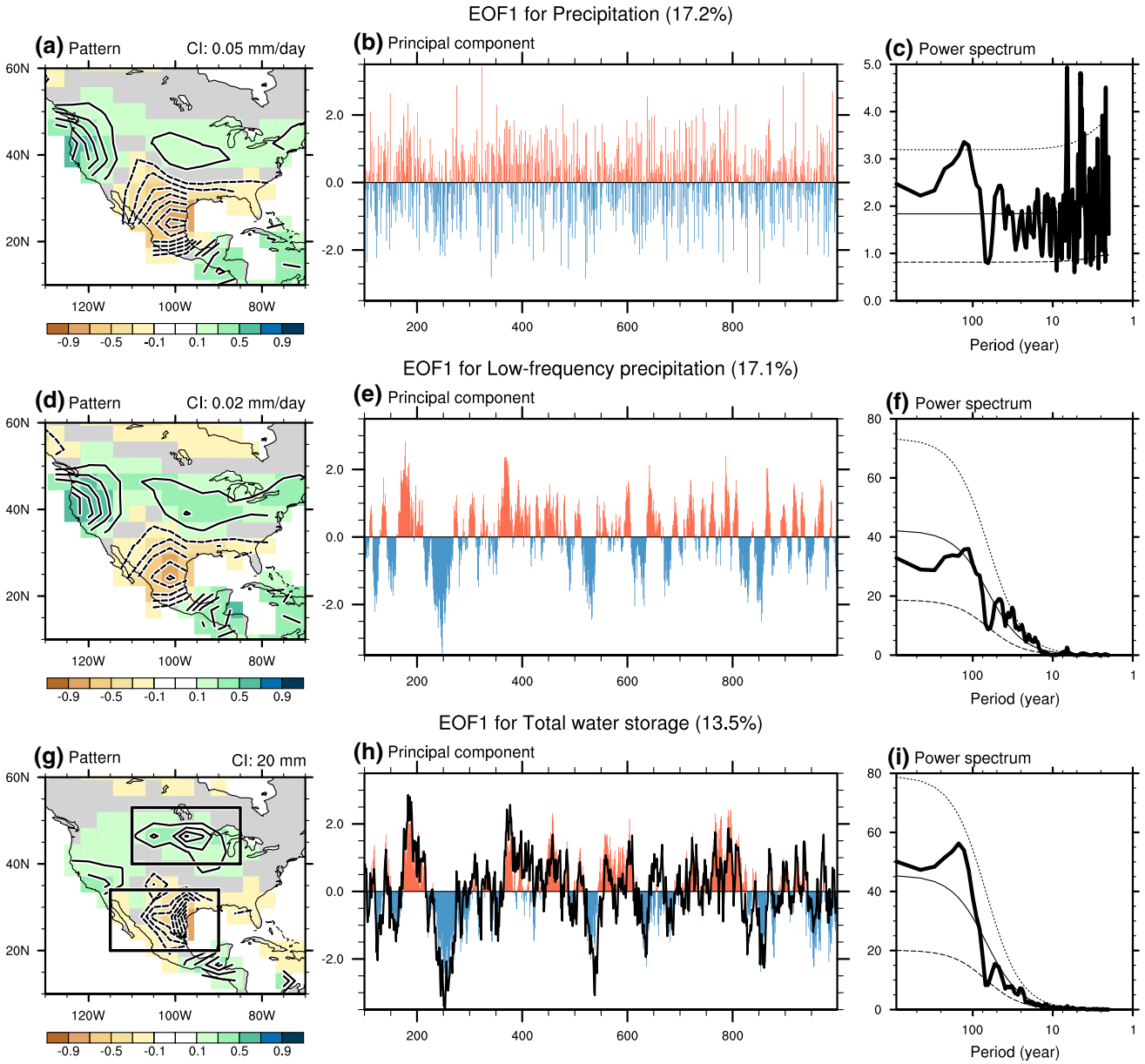

Fig. 4 First EOF modes for precipitation (*top panels* **a**–**c**), 10-year running mean precipitation (*middle panels* **d**–**f**), and total water storage (*bottom panels* **g**–**i**). *Left*, *center*, and *right panels* indicate correlation (*color*) and regression maps (*contour*) for principal components, normalized time series, and power spectrum for these first EOF modes, respectively. Contour intervals are shown in the *upper-right corner* in the *left panels*. Zero contours are omitted. *Solid*, *dotted*, and *broken lines* in *right panels* (**c**, **f**, **i**) correspond to a power spectrum of a fitted 1st order Markov process and its 95 and 5 % confidence limits, respectively. *Solid line* in (**h**) represents time series estimated by 1st order Markov process using the precipitation noise of (**b**)

Figure 5 shows correlation maps of zonal wind variability in the upper and lower level troposphere associated with the first EOF modes in Fig. 4. We find that the precipitation variability over North America is closely related to a narrowing of the midlatitude jet. High precipitation conditions in northwestern US and drought conditions in the southwestern US are associated with increased 200 and 850 hPa winds along the west coast of the US and weaker winds straddling both sides of the wind anomaly maximum. Owing to the similarity of the principal components of the different variables in Fig. 4, this narrowing of westerly jet downstream plays an important role in generating hydroclimate variability on all timescales over North America. These results support the notion that the leading pattern of total water storage in North America is determined to first order by the downstream jet flow activity (Seager et al. 2010).

Many observational studies have documented the relation between decadal to multi-decadal-scale droughts in the

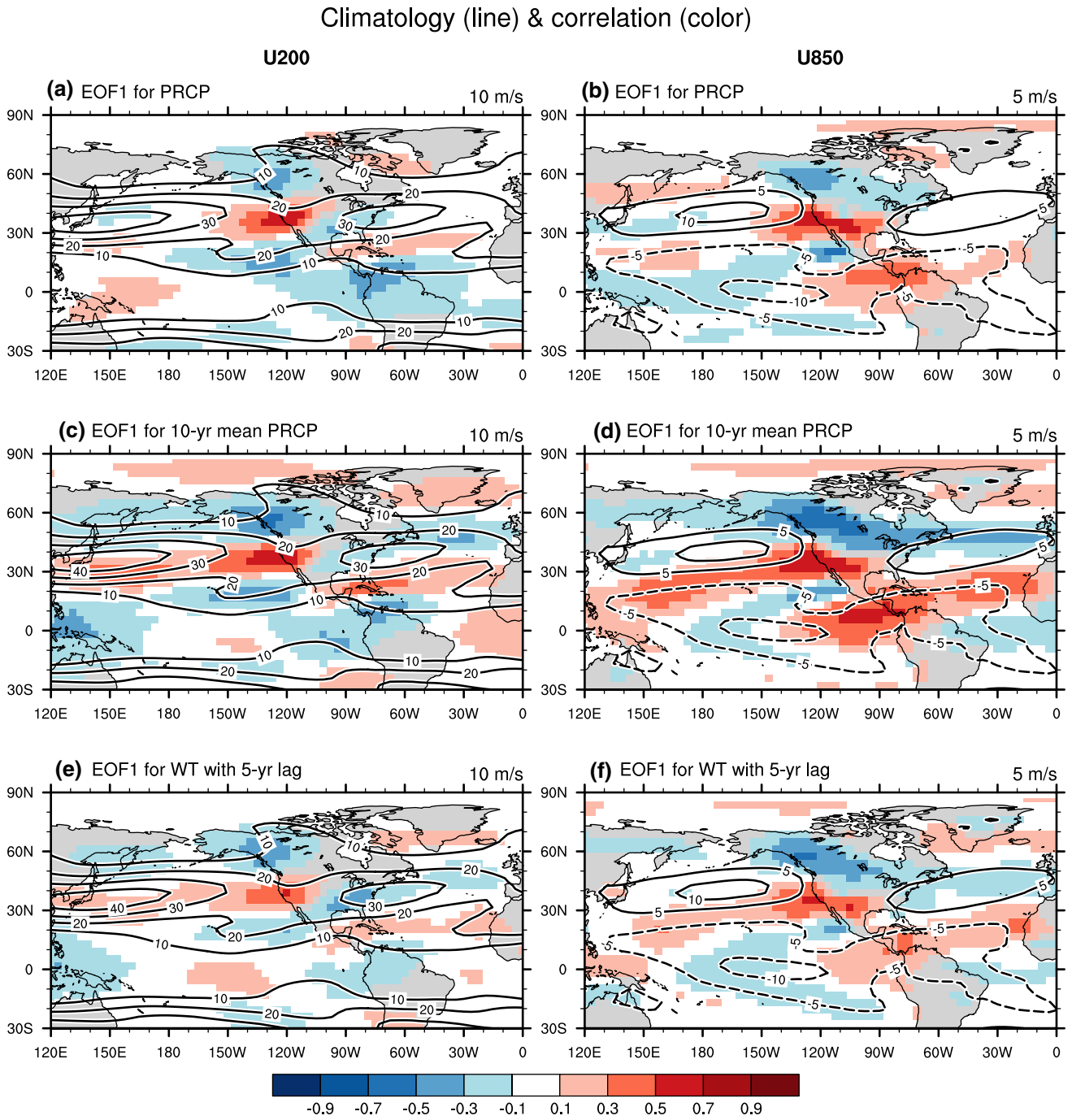

Fig. 5 Correlation maps (*shaded*) of zonal winds at 200 and 850 hPa associated with the first EOF modes of annual precipitation (**a**, **b**), low-frequency precipitation (**c**, **d**), and total water storage (**e**, **f**). Correlation coefficients are calculated using annual mean data for the first EOF mode of annual precipitation, 10-year running mean data for the low-frequency precipitation, and 10-year running mean data leading with 5-year for the total water storage. Contours represent annual climatology of zonal winds and zero contours are omitted

US and leading modes of sea surface temperature (SST) anomalies, such as the Pacific Decadal Oscillation (PDO), the Atlantic Multidecadal Oscillation (AMO) (Seager et al. 2005, 2008; Meehl and Hu 2006; Sheffield and Wood 2008; Schubert et al. 2009; Famiglietti et al. 2011; Dai 2011; Hu et al. 2013), and ENSO (Kanamitsu et al. 2003; Barlow et al. 2001; Chen and Kumar 2002, 2004; McCabe et al. 2008; Dai 2013). To determine the relation (not the causality) between SST and simulated decadal hydroclimate variability in the CESM CTL run, we calculated the correlations and regressions of the SST and sea level pressure (SLP) anomaly fields with the leading principal

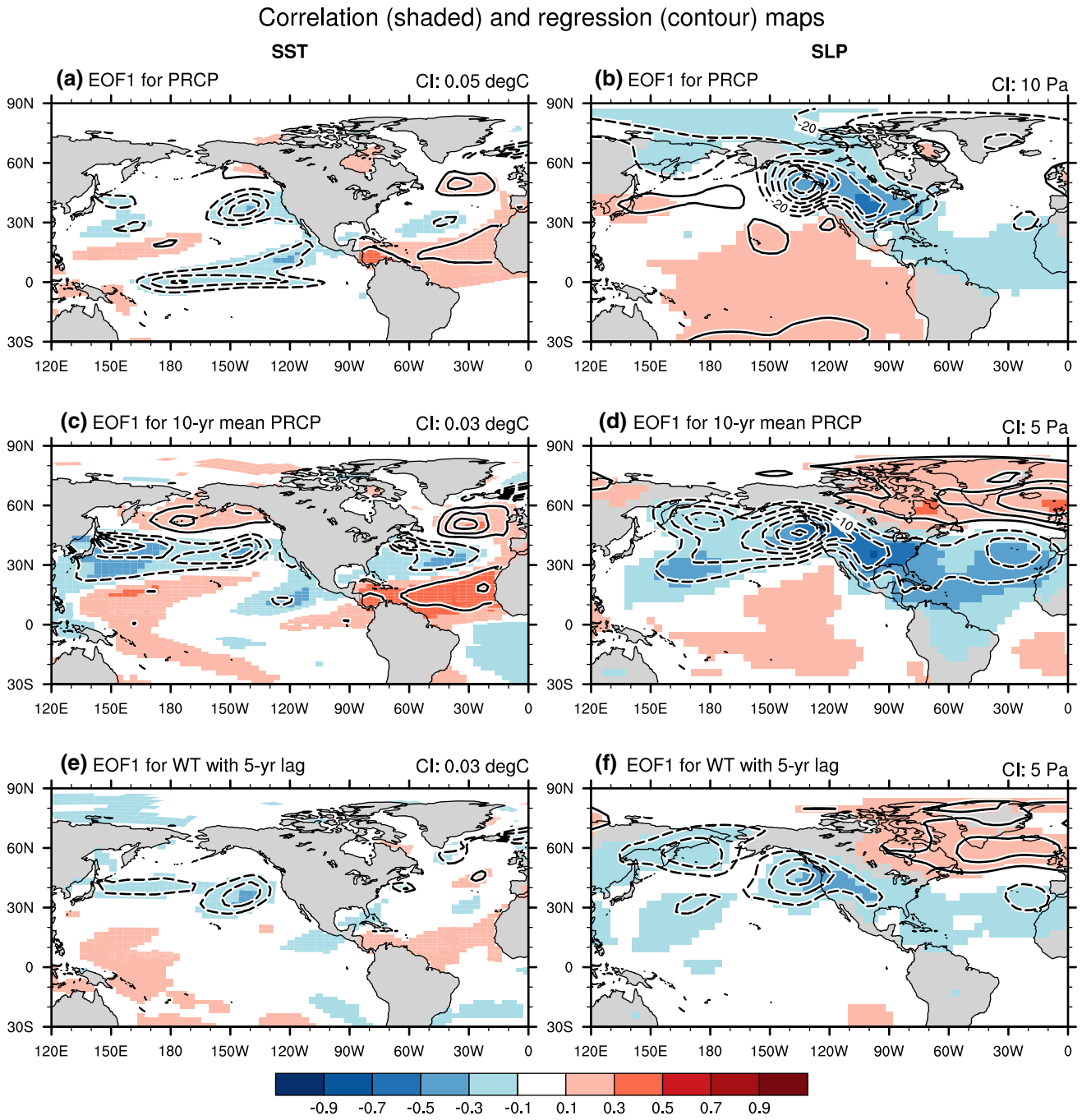

Fig. 6 Correlation (*color*) and regression maps (*contour*) of SST (*left*) and SLP (*right*) associated with the first EOF modes of annual precipitation (**a**, **b**), low-frequency precipitation (**c**, **d**), and total water storage (**e**, **f**), which are calculated using annual mean data for the first EOF mode of annual precipitation, 10-year running mean for precipitation, and 10-year running mean leading with 5-year for total water storage. Contour intervals are denoted in the *upper-right corner* in each panel. Zero contours are omitted

components in Fig. 4. The analysis shows that decadal-scale precipitation variability over North America correlates with anomalous SSTs in the Kuroshio/Oyashio extension region (Fig. 6c). These SST anomalies also correlate with the leading principal component of the total water storage (Fig. 6e) although its amplitude is much smaller than those associated with the decadal precipitation variability. This is because the decadal precipitation variability is directly coupled with SST and SLP anomalies as a part of atmosphere-ocean interactions, whereas total water storage changes indirectly relate to SST and SLP variability through the land hydrological processes. Previous studies

(McCabe-Glynn et al. 2013) have also invoked statistical links between US droughts and warmer conditions in the Kuroshio/Oyashio extension region, however its dynamical connection is still unclear.

In the Atlantic, we find that enhanced rainfall in the northeastern US is also accompanied by a reduction of the trade winds and westerlies (Fig. 5), reminiscent of a weakened North Atlantic Oscillation (NAO). The first EOF mode of low-frequency precipitation variability over North America is accompanied by a negative NAO mode in SLP (Fig. 6d). As already shown by Bjerknes (1964), NAO-related heat fluxes cause a tripole-like SST pattern, similar to the one shown in Fig. 6c. These SST and SLP patterns around the North America also appear in the regression maps derived from the leading principal components of total water storage (Fig. 6e, f). It remains uncertain what role Atlantic SST anomalies play in generating the low-frequency Pacific wind response and the simulated North American precipitation anomalies in CTL. Recent studies document the effect of Atlantic SST variability on global climate anomalies, including rainfall changes over North America, via trans-basin adjustments of the global Walker Circulation (Chikamoto et al. 2012; McGregor et al. 2014).

Determining whether SST anomalies are key drivers for multi-year jet activity, or whether they merely respond to random internal atmospheric variability is beyond the scope of this study. The relative roles of SST-driven and stochastically generated precipitation changes over North America are examined in more detail in companion studies (Langford et al. 2014; Stevenson et al. 2014).

3.2 Higher EOF modes for precipitation and total water storage

The leading EOF mode reveals a clear relationship among precipitation, total water storage, and the downstream activity of the westerly jet. However, this relationship becomes less evident for the higher order EOF modes. In fact, when we apply the simplified conceptual model to the second principal component of annual mean precipitation (Fig. 7), we find the weaker relationship compared to the leading mode (Table 1); correlation coefficients of 0.76 and 0.66 in the first and second EOF modes, respectively. As for the third EOF mode (not shown), the correlation coefficient becomes zero (Table 1).

The second EOF mode of total water storage explains about 10 % of the variance and is characterized by strongly pronounced multidecadal to centennial variability (Fig. 7h, i). In contrast, this pronounced low-frequency variability has disappeared from the second precipitation mode (Fig. 7b, c). On interannual to decadal timescales, however, these second principal components of precipitation and total water storage significantly correlate with each other, attaining values of 0.42. Comparing the EOF patterns in Fig. 7 with Figs. 2 and 3, it becomes evident that the second mode of hydroclimate variability over North America is largely driven by an atmospheric circulation pattern (the Pacific North American pattern; not shown) that also gets excited during El Niño events. Indeed, the Niño 3.4 index has a statistically significant correlation of 0.33 with the second principal component of annual mean precipitation, which is considerably higher than that with the first EOF mode (Table 2). Even though the second EOF modes of precipitation and water storage bear interesting dynamics, we will focus our further analysis on the meridional jet mode characterized by EOF1 (Fig. 4), which explains about 5 % more variance than the second mode.

3.3 Potential predictability of land hydrology

The relationship between precipitation and total water storage variability shown above suggests that, in spite of the white noise characteristics of precipitation anomalies over North America, the total water storage has long-term predictability due to the natural low-pass filter effect of soil and aquifer. In the real climate forecast, however, the atmospheric random noise usually dismisses climate predictive skills. According to the statistical theory, we can reduce this atmospheric random noise by applying the ensemble approach to the prediction. To evaluate the upper limits of predictability for land-surface hydrology on interannual to decadal timescales, therefore, we conducted a suite of 10-member ensemble perfect model hindcast experiments with CESM for 39 different initial conditions, as described in Sect. 2. Focusing only on the first EOF mode of total water storage (Fig. 4g), we define the Northern US and Southern US/Mexico index regions (see box outlines in Fig. 4). As expected from the meridional seesaw pattern in Fig. 4g, the total water storage variability of the pre-industrial control simulation (black in Fig. 8) exhibits out-of phase low-frequency variability between these two index regions. Consistent with this low-frequency variability, the 10 member hindcast ensemble tracks the simulated hydrological changes in the control run (thick red and blue lines for ensemble mean and pink and light blue shadings for ensemble range in Fig. 8a, c, and e). This behavior translates into a high degree of predictability, as measured here by the anomaly correlation calculated for all initial conditions between the ensemble mean hindcast of water storage for the respective index regions and the control run (Fig. 8b, d, and f).

The tendency for water storage anomalies to relax back to climatological values (zero anomaly) on timescales of several years is illustrated here for an initial condition picked in model year 240 (Fig. 9). At the initial time in 240, total water storage anomalies are negative in northern

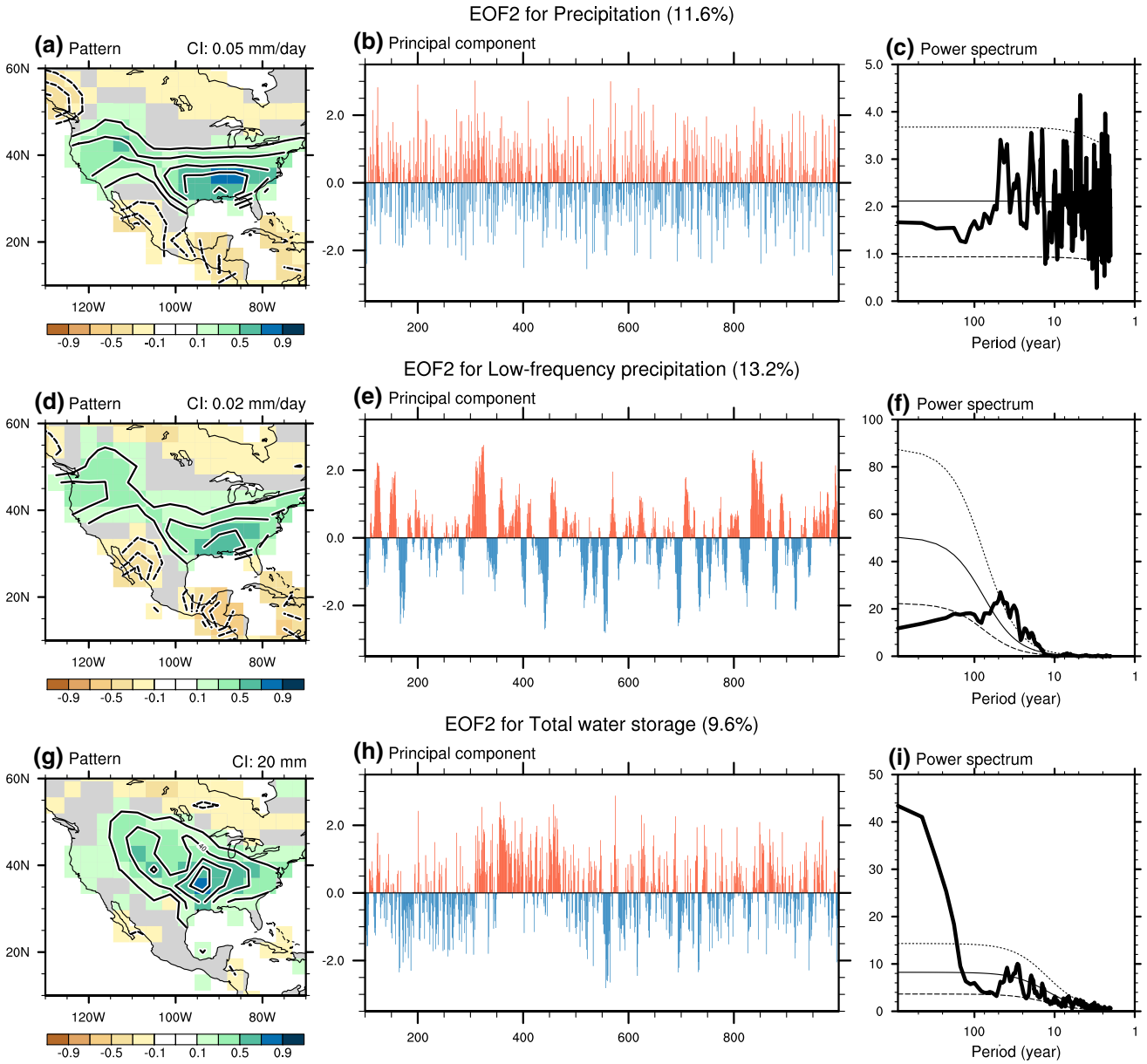

Fig. 7 Same as Fig. 4, but for the second EOF mode

Table 1 Correlation coefficients between the principal components of EOF modes for total water storage (Figs. 4h, 7h) and the time series estimated by 1st order Markov process using the precipitation noise (Figs. 4b, 7b)

EOF1	EOF2	EOF3
0.76	0.66	0.00

US but positive in southern US/Mexico region, thus featuring an enhanced meridional gradient (Fig. 8a, c, and e). The ensemble mean prediction in the hindcast run initially captures the meridional gradient and drought conditions over central America simulated in the CTL run (Fig. 9a, b). For increasing lead times, this meridional gradient gradually decays in the hindcast run (Fig. 9d, f), contrasting with the evolution in the CTL run. However, the ensemble mean in the hindcast run fails to capture further drying over California and increasing rainfall over Mexico in CTL run because of the unpredictable atmospheric component: a prominent positive SLP anomaly over the northern US (Fig. 9c, e), which resembles the regression pattern in Fig. 6b. The behavior illustrated here for water storage is typical for a 1st order stochastic Markov process described by Eq. (3): predictions started from given initial conditions relax back toward climatology with a damping timescale of λ^{-1}.

Table 2 Correlation coefficients of the principal components of the three EOF modes for annual mean precipitation (Figs. 4b, 7b) with the Niño 3.4 index

PC1	PC2	PC3
−0.17	0.33	0.08

To further elucidate at what soil depth multi-year predictability emerges, we calculated, for different depth ranges, the anomaly correlation skill between the CTL run and the ensemble mean for the two geographic index regions. The results show that the predictive skill in the northern US increases rapidly for soil levels below 1 m (Fig. 8b). For the southern US/Mexico, even precipitation and upper soil levels exhibit predictive skill of up to 2–3 years (Fig. 8d). The skill of the difference of these indices also exhibits a similar depth dependence (Fig. 8f). To compare our CESM results with the damped persistence of a simple 1st order Markov model, we conducted a 10,000 member Monte Carlo linear 1st order Markov model hindcast (Eq. 3), using a depth-dependent damping timescale estimated from the control simulation and initialized for the same initial conditions as the CESM hindcast experiments. The resulting anomaly correlation skill is depicted by the black circles in Fig. 8b, d, and f. We find a close agreement between the CESM-based hindcasts and the Markov model, indicating that the largest contribution to the predictive skill of soil water on interannual to decadal timescales in CESM can be attributed to the damped persistence, which is partly governed by the evapotranspiration (Delworth and Manabe 1988), the total runoff, and the diffusion of soil moisture into the deeper soil levels as shown in the Eq. (2). As a result of these processes, the predictability for both the Markov model and CESM model hindcasts increases with depth attaining values of up to 5–8 years for the northern US and 10 years for the southern US/Mexico index regions.

The key result from our analysis is that although precipitation variability is statistically not predictable beyond 1–2 years in our model, soil moisture variations at deeper soil levels and total water storage (including aquifers) in the northern US and southern US/Mexico regions can be predicted up to a decade ahead. The longer persistence of soil water properties can be explained by the stochastic drought model concept captured by Eq. (3). Our results with a comprehensive coupled earth system model confirm earlier results from Delworth and Manabe (1988) that were based on a coupled land-atmosphere model forced by varying SST anomalies on interannual timescales. Our study has identified soil water predictability even beyond the interannual timescales, thus extending the potential predictive range of hydrological conditions over North America to almost a decade. In the next section, we will explore the impact of decadal soil water changes on fire frequencies and simulated vegetation changes over North America.

4 Decadal predictability of fire risk linked to hydroclimate

The CESM CTL and hindcast experiments are further used to determine the interactions between soil water, fire, and vegetation and potential long-term predictability emerging from these interactions. The carbon biogeochemical cycle in CLM4 calculates changes in vegetation and wildfire occurrences, both of which depend on hydrological conditions (Thonicke et al. 2001; Kloster et al. 2010). The fire parameterization in CLM4 assumes that the annual carbon fraction burned every year is a function of annual fire season length that is defined as the sum of probability of at least one fire in a day over the whole year (Thonicke et al. 2001). This assumption is valid in the relatively large grid box as provided by our low-resolution land model. Therefore, changes in fire frequency correspond to those in the fire season length in our model. As fire probability is parameterized in terms of soil moisture in the upper 5 cm and fuel-availability, dry soil conditions can enhance the fire frequency directly (Viegas et al. 1992). An enhanced fire season length reduces primary productivity and the terrestrial carbon stock in the grid cell, which in turn feeds back to the soil conditions via evapotranspiration and other processes (Bowman et al. 2009). Although droughts can cause hydrological conditions that favor wildfires, they can also suppress wildfire occurrences by reducing vegetation carbon stocks and hence the fuel-availability necessary for the ignition of wildfires (van der Werf et al. 2004; Lehmann et al. 2014). This complex interplay between soil hydrology, fire, and vegetation may have potential predictability on multi-year timescales and will be referred to as a *fire cycle*.

To illustrate the interplay between variations in fire occurrences and low-frequency soil water variability, we show simulated standardized timeseries of total water storage, total vegetation carbon, and the computed fire season length (Fig. 10) for the Northern US and the Southern US/Mexico regions defined in Fig. 4. We find in both regions that all variables exhibit low-frequency variability on decadal to multidecadal timescales. In the Northern US, for instance, persistent dry soil conditions around model years 250, 520, and 700 are associated with increased fire season length and reduced terrestrial carbon stocks (Fig. 10a, c). Both the increased fire season length and the low soil moisture conditions contribute to the low vegetation carbon and reduce primary production. A long-lasting pluvial during years 350–500 in the Northern US decreases fire frequency and enhances total vegetation carbon (Fig. 10a, c). In this region, the fire season length is controlled by the

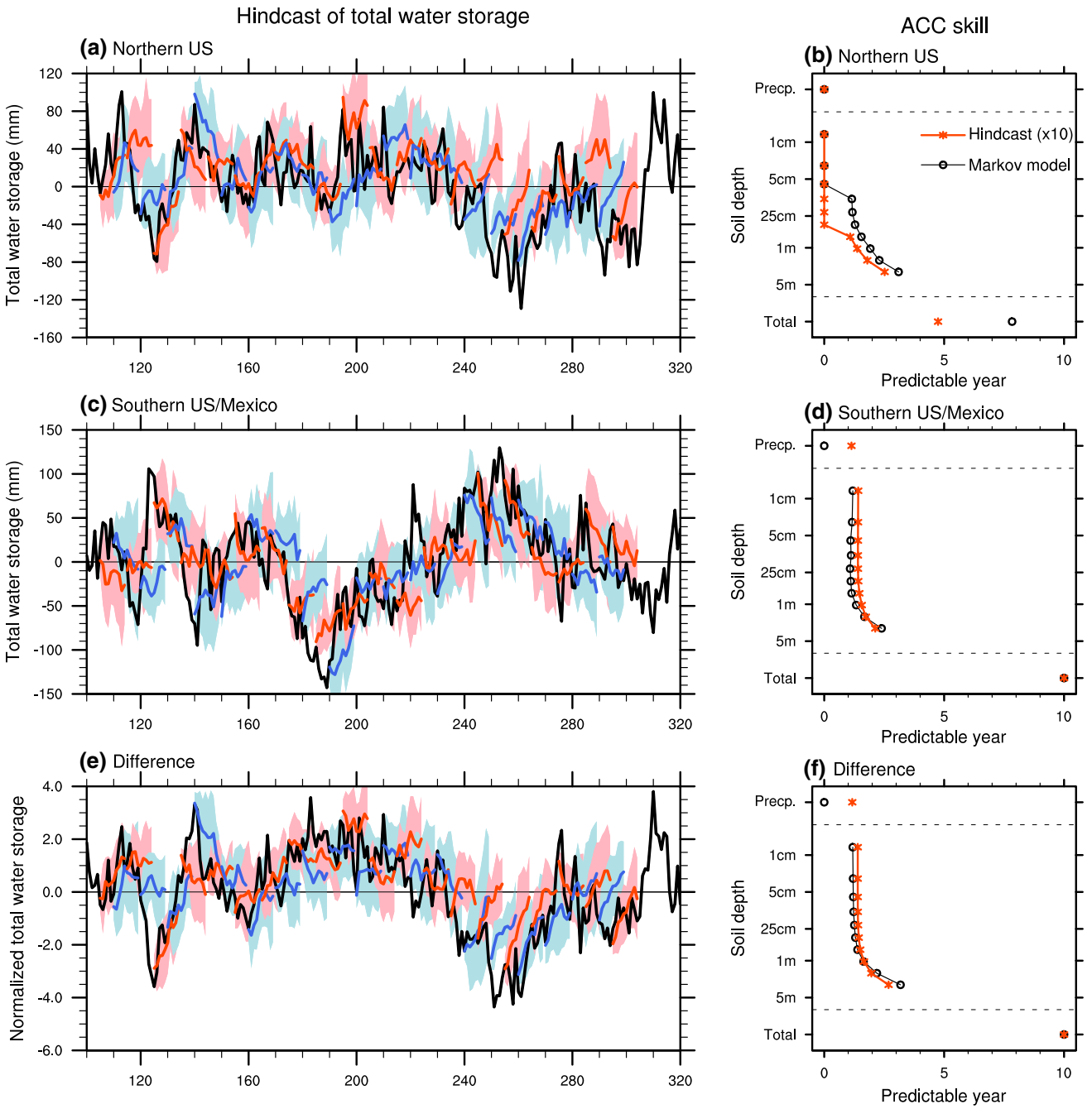

Fig. 8 Time series of total water storage averaged over **a** the northern US, **c** the southern US/Mexico, and **e** the difference of these indices (see boxes in Fig. 1g for index regions) in the pre-industrial control simulation (*black line*) and the hindcast experiments. *Colored lines* and *shadings* show the ensemble mean prediction and the ensemble spread of the predictions; drawing *red* and *blue* alternately evey 5 years. *Right panels* show the predictability horizon for annual mean precipitation (above the *dashed line*), soil water averaged from the surface, and total water storage (below the *dashed line*), estimated from the 39 individual 10 member hindcast experiments (*red*) and the 1st order Markov model with 10,000 ensemble members (*black circle*) for the **b** the northern, **d** southern, and **f** these difference indices. The predictability horizon corresponds to the time interval when the anomaly correlation coefficient exceeds the 99 % significance level using 37 degrees of freedom (correlation coefficient is 0.37)

soil moisture conditions rather than by the fire-fuel availability, as manifested by the negative correlation between fire frequency and vegetation (Fig. 11a). The Southern US/Mexico region also shows a similar relationship, but weaker correlation coefficients among these three variables (Figs. 10, 11) and a reduced persistence in the system.

An important difference arises between these regions in terms of soil water/vegetation coupling. Soil water

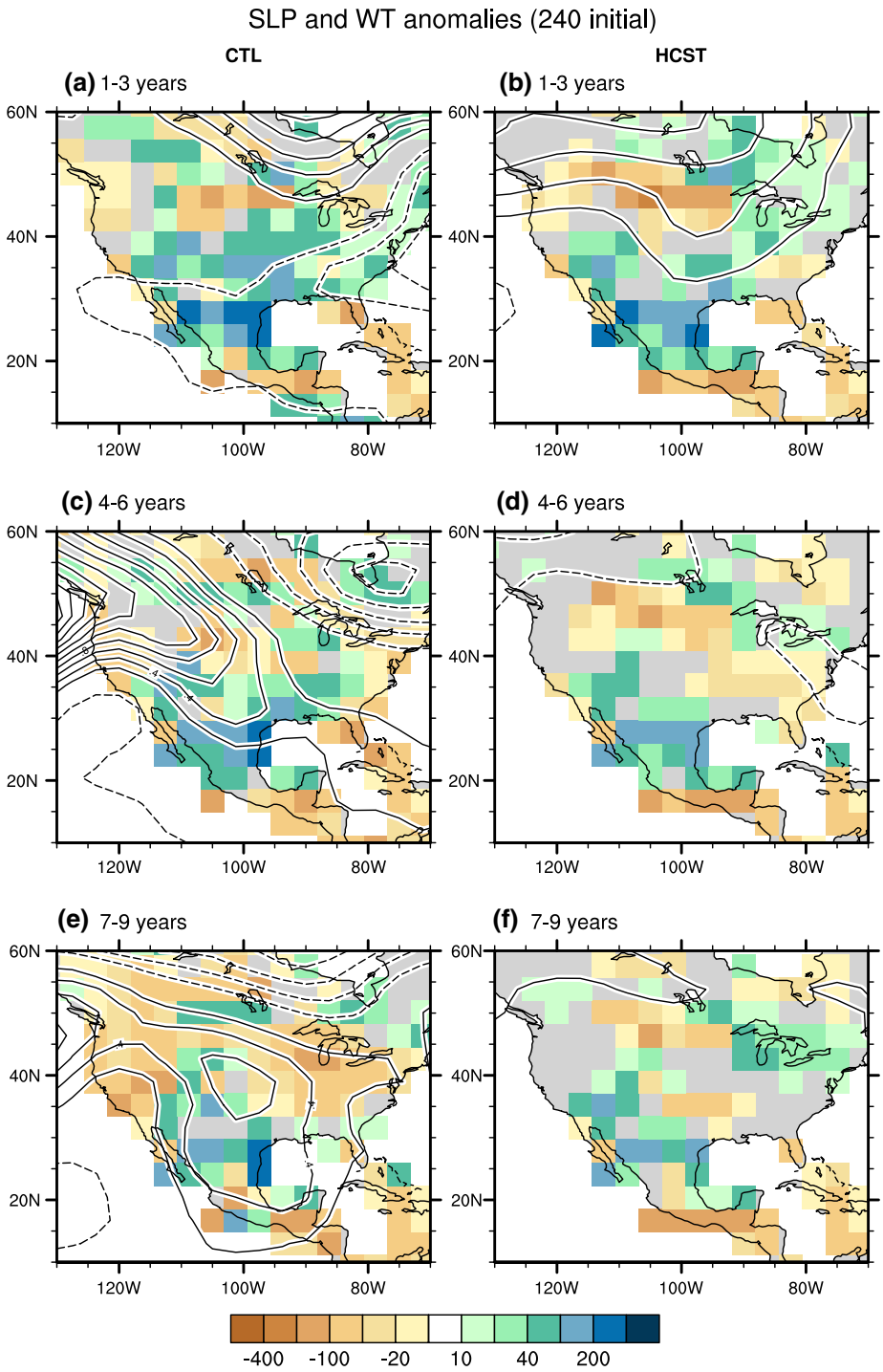

Fig. 9 Temporal evolution for three-year-mean anomalies of SLP (*contoured*) and total water storage (*shaded*; units are mm) in CTL and the ensemble mean of hindcast run initialized in 240. The 3-year-mean anomalies correspond to **a**, **b** 240–242, **c**, **d** 243–245, and **e**, **f** 246–248 model years in CTL run or 1–3, 4–6, and 7–9 years lead in the hindcast experiment. The contour interval of SLP anomalies is 0.2 hPa and the zero contour is omitted

variations in the Northern US are more tightly coupled with vegetation variability than in the Southern US/Mexico index region. This leads to different dynamics of the regional fire cycles: In the Northern US, negative correlations of fire with water storage or vegetation for negative lags (fire leads) suggest that the enhanced fire frequency will reduce vegetation carbon and affect subsequent droughts lasting for several years. The absence of a statistically significant correlation for positive lags (vegetation and soil water lead) indicates that soil moisture and vegetation are not precursors for fire season length on decadal timescales. Even though correlations for the Southern US/Mexico area average are low, we observe a sign change in the correlation between vegetation and fire for positive (fire lags) versus negative lags (fire leads). For positive lags, the increasing vegetation builds up fuel and increases

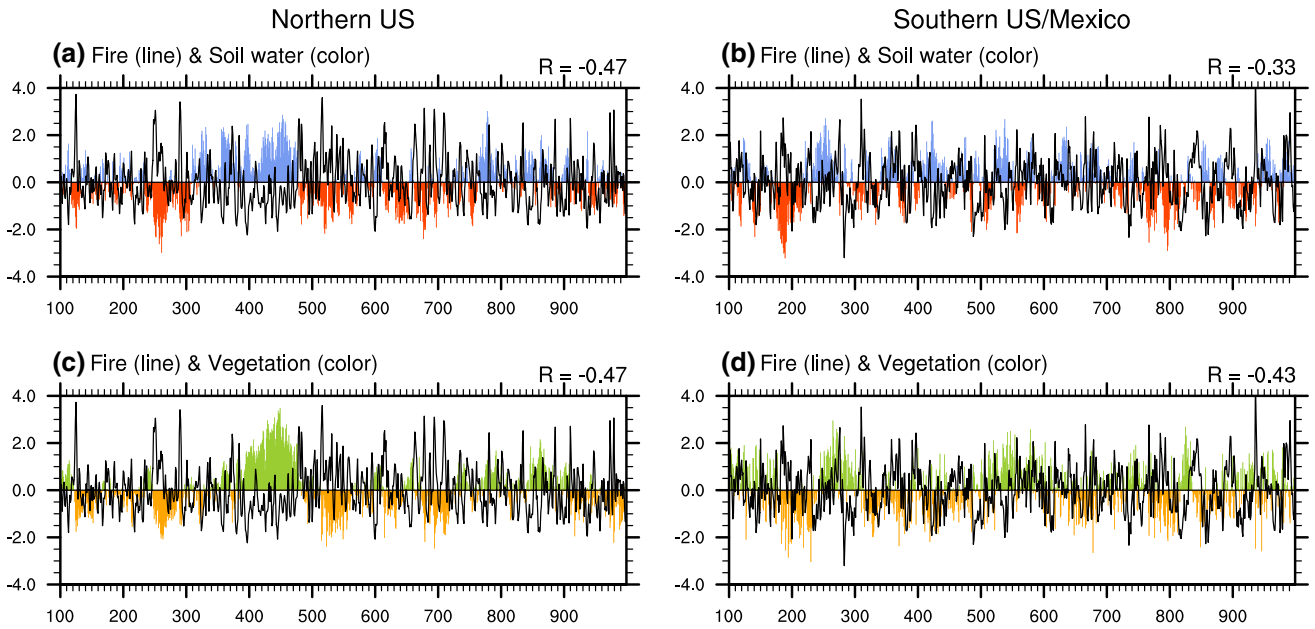

Fig. 10 Time series of total water storage (*color* in *upper panels*), fire season length (*lines* in *upper* and *bottom panels*), and total vegetation carbon (*color* in *bottom panels*) averaged over the Northern US and Southern US/Mexico regions in the pre-industrial control simulation. Time series are normalized by standard deviations of each variable. Correlation coefficient between two timeseries in each panel is shown by *upper-right corner*

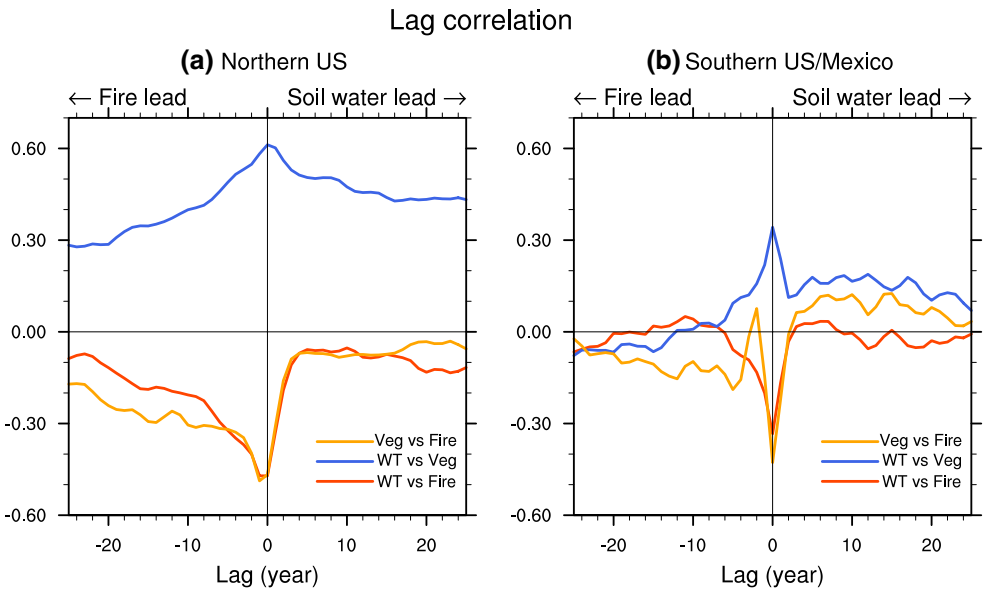

Fig. 11 Lead-lag correlation between variations in annual mean total water storage, total vegetation carbon, and annual fire season length over the Northern US and the Southern US/Mexico regions in the control simulation. *Blue* and *red lines* represent lag correlation coefficients of total water storage with total vegetation carbon and annual fire season length (total water storage leads in the positive lags). The *orange line* corresponds to the lag correlation coefficients between the total vegetation carbon and the annual fire season length (vegetation leads in the positive lags). Correlation coefficient of 0.20 corresponds to the statistical significance at the 95 % level by using a two-side Student *t* test with 100 samples

fire risk. For negative lags, the increased fire leads to reduction in the vegetation carbon. This will be further interpreted below for specific grid points.

To evaluate the decadal predictability of fire variability, we compute the predictive skill for 1, 2–5, and 6–9 years lead time using the ensemble hindcast experiments

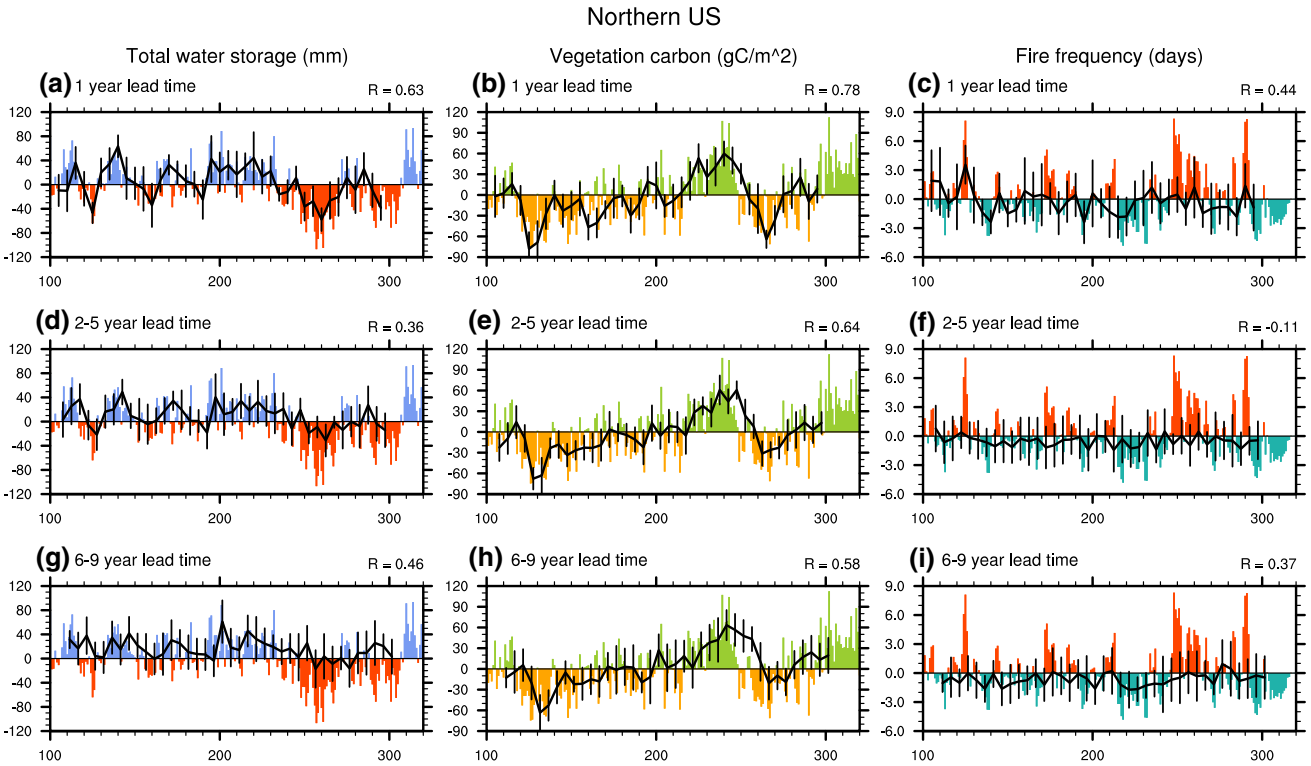

Fig. 12 Decadal climate prediction of annual mean variations in total water storage (*left*), vegetation carbon (*center*), and fire season length (*right panels*) over the Northern US. *Color bar* and *solid line* denote the control simulation and the hindcast experiment, respectively. *Error bars* capture the ensemble spread (one standard deviation) in the hindcast experiment estimated from 10 ensemble members. Correlation coefficients between the control and the hindcast experiments are represented in the *upper-right corner* of each panel, which corresponds to the predictive skill

analyzed in Sects. 2 and 3. Based on the analysis of the CTL experiment alone, we can already expect considerable predictive skill of decadal variations in fire season length and vegetation carbon. Figures 12 and 13 show the predictions (ensemble mean and the ensemble spread) for total water storage, vegetation carbon, and fire season length. In the Northern US, we find high predictive skill on lead times of up to 6–9 years for total water storage (see Figs. 8, 12a, d, and g) and vegetation carbon (Fig. 12b, e, and h). In spite of the high skill for these variables, the anomaly correlation skill for the annual mean fire season length drops down quickly after one year lead time (Fig. 12c, f, and i). This is consistent with the low correlation values for positive leads in Fig. 11a. In the Southern US/Mexico region, we find high predictive skills for lead times of 6–9 years for total water storage and vegetation carbon and also for the fire season length (Fig. 13). Clearly, time-series of fire frequency for model years 100–340 exhibits more low-frequency variability in the Southern US/Mexico (Fig. 13c) than the corresponding time in the Northern US (Fig. 12c). This difference may explain the increased persistence of the system and the higher predictability in the Southern US/Mexico region. As demonstrated below, this low-frequency variability is largely governed by a few grid points that exhibit a fire/vegetation oscillation.

To further study how potential predictability in fire season length would translate into estimates of fire risk, we calculate how ±1 standard deviation anomalies in total water storage, if predicted successfully, would affect the simulated probability distribution of fire season length in the Northern and Southern US/Mexico index regions (see boxes in Fig. 4g). Drought conditions (dashed histogram in Fig. 14) cause a significant shift of the histogram of fire season length compared to climatological conditions (gray shading in Fig. 14) and the wetter situation (solid histogram in Fig. 14). Whereas shifts in the mean fire season length amount to only about 10 days, the probability for extreme values increases markedly for dry conditions (Fig. 14c, d). In Southern US/Mexico, we find that the probability to have extreme anomalies of fire season length of ∼30 days increases fourfold for dry conditions. For pluvials, the change to have fire seasons of 30 days less than the climatology increases sixfold. Although the linear-based predictive skill of fire frequency is limited to 1 year in the Northern US (right panels in Fig. 12), this method would still allow for probabilistic estimates of extreme fire

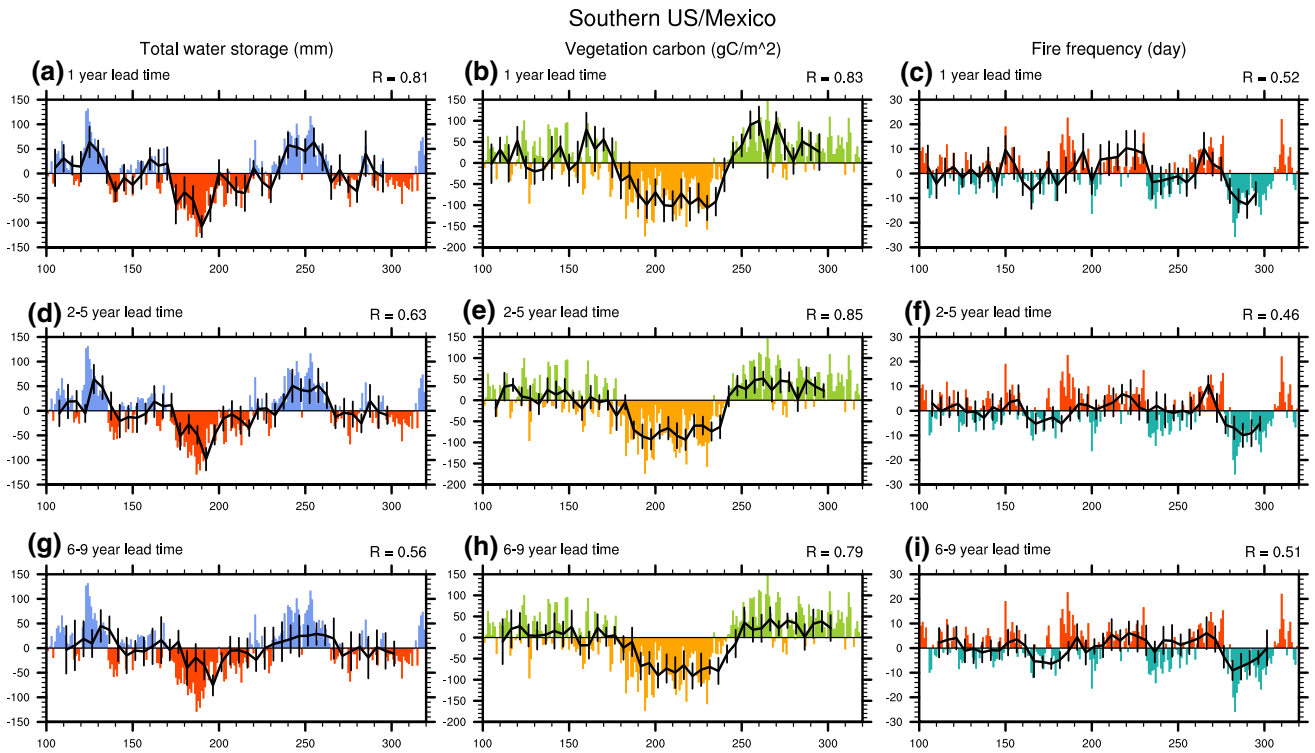

Fig. 13 Same as Fig. 12 but for the Southern US/Mexico region

risks several years ahead, if the soil water conditions were predicted accurately.

Figure 15 shows a spatial distribution of the anomaly correlation coefficients (ACC) between control run and hindcast ensemble means for various lead time (1, 2–5, and 6–9 years). We find that total water storage is highly predictable over large areas of Southern California (San Diego and Los Angeles area). Weaker but still considerable predictive skill is found west of the Great Lakes and in Central America. As a result of the very slow decadal-scale growth timescales of vegetation, total vegetation carbon is a highly predictable variable with high anomaly correlation values exceeding 0.6 for most of North America even for lead times of 6–9 years. After a major disruption, such as massive fire, vegetation needs several decades to grow back to its equilibrium value, thus translating into very long damped persistence and high predictive skill.

On average the fire frequency loses predictive skill quickly over North America after about 1 year lead time. However, there are some interesting exceptions. Several grid points in Central America and Southern California exhibit excellent predictability event beyond the 6–9 year predictability horizon considered here. A more detailed view of the underlying dynamics is given in Fig. 16. For instance, a grid point near Los Angeles with high predictive skill in Fig. 15 shows very regular oscillatory behavior in vegetation carbon and fire season length with a period of about 60 years (Fig. 16d). This fire-vegetation cycle is based on the following dynamics: Increasing vegetation carbon leads to an increase in fire fuel. Reaching a fire threshold in this already dry areas, a rapid increase of fire frequency subsequently diminishes vegetation carbon. As a result of reduced supply of fuel, fire frequencies drop rapidly and the vegetation has time to regrow until the carbon storage reaches the threshold. This behavior, which leads to a typical relaxation oscillation, is well captured in the lag correlation between vegetation and fire (Fig. 17b). Correlations involving soil water storage are insignificant, indicating that for this dry grid point, the limiting factor is carbon (fuel) rather than soil water.

The relaxation oscillation of these grid points can be contrasted with a different fire/vegetation/soil moisture regime found in a grid point in Montana ("S" mark in Fig. 15). We see that for this location the fire activity is modulated by the soil water variability rather than by the vegetation carbon stock because the fire shows much more high frequency variability compared to the vegetation and strongly correlates with the total water storage rather than with the vegetation (Fig. 16a, c). In addition, correlation coefficients between total water storage and total vegetation carbon are higher for positive lags than negative ones (Fig. 17a), which is indicative of the effects of soil water on vegetation, but not vice versa.

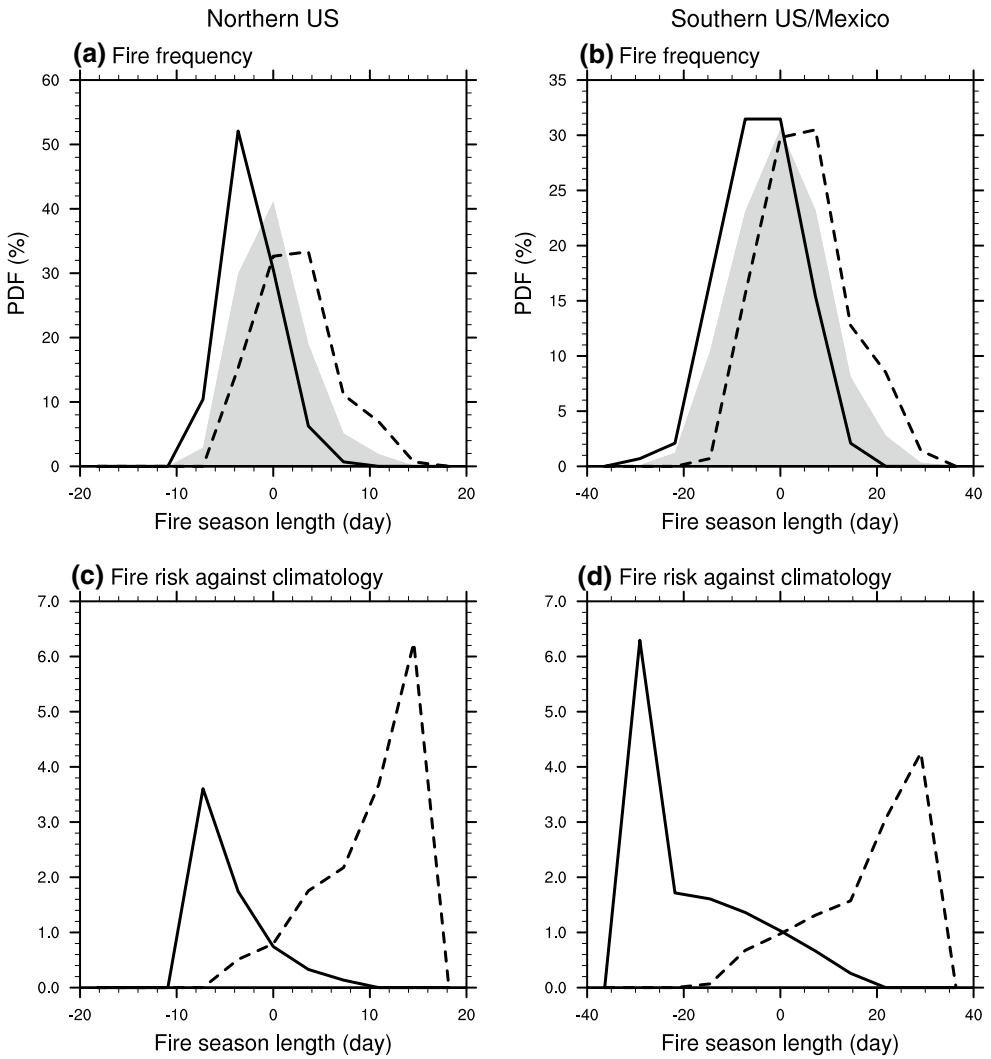

Fig. 14 Normalized histograms of the annual mean fire seasonal length (*top*) and fire risk (*bottom*) over the northern (*left*) and southern North American (*right*) index regions (see *boxes* in Fig. 1g) from the pre-industrial control simulation. *Solid* and *broken lines* show histograms for total water storage below and above one standard deviation, respectively. *Gray shading* represents the normalized histogram calculated from the entire 900-year-long pre-industrial control simulation. Fire risk is evaluated from the histogram ratio of wet (*solid*) or dry (*broken*) conditions to the entire period (*gray* in *top panels*)

5 Discussion

We have studied the underlying dynamics and potential predictability of decadal-scale variations in soil water, vegetation, and fire frequency over North America using a pre-industrial control simulation conducted with the low resolution version of CESM. Our study has been motivated by the finding of decadal-scale persistence of drought conditions over North America (Woodhouse and Overpeck 1998; Stahle et al. 2007; Dai 2011) and low-frequency characteristics of fire cycles (e.g., Swetnam and Betancourt 1998; Westerling et al. 2003; Brown et al. 2005; Farris et al. 2010), as reconstructed from lake sediments and fire-scar. Based on the *perfect* model framework, our results provide estimates of the maximum potential predictability of soil hydrological variability. We demonstrated by comparing the CESM predictions with simple 1st order Markov models that most of the land surface predictability in the CESM experiments results from the integrative effect of soils and the slow adjustment processes of vegetation in response to climatic and fire-related disturbances. Thus, actual decadal forecasting of soil water, vegetation, and fire frequencies would require initialization of observed water content in soil and aquifer.

It should be noted that our predictability estimates are based on the perfect model assumption and are hence very likely to be overestimates of the real predictability of the coupled climate-land-vegetation system. On the other hand,

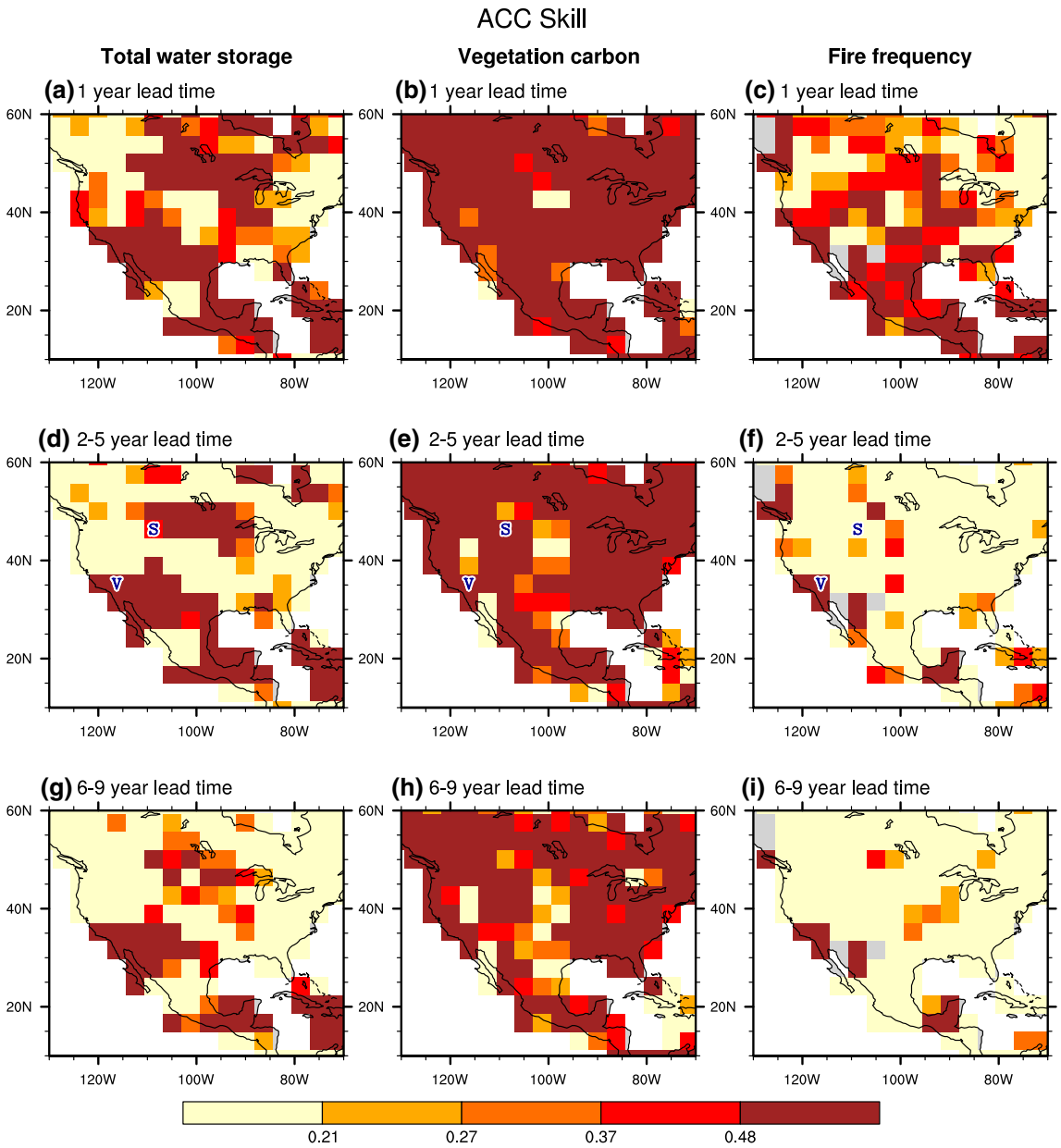

Fig. 15 Decadal climate predictability of annual variations in total water storage (*left*), total vegetation carbon (*center*), and fire season length (*right*) in the North America for 1 (*upper panels* **a**–**c**), 2–5 (*middle panels* **d**–**f**), and 6–9 years lead time (*bottom panels* **g**–**i**). Correlation coefficients of 0.21, 0.27, 0.37, and 0.48 correspond to the statistical significant levels at 90, 95, 99, and 99.9 % with 37 degrees of freedom with one-tail Student's *t* test

the anthropogenic component and the aerosol forcing, which were neglected in our study, may induce additional predictable trends. Furthermore, SST variability (Seager et al. 2005, 2008; Meehl and Hu 2006; McCabe et al. 2008), as well as external forcings (Dai 2011, 2013; Coats et al. 2013), may contribute to the low frequency variability and potential decadal-scale predictability of hydroclimate variability over North America. Other factors that will affect the forecast skill of a realistically initialized CESM include ensemble size, internal model biases, initialization method, and the low resolution adopted here. In particular, larger ensemble sizes may help improving the predictive skill of total water storage in the Southern US/Mexico region where the climate model hindcast slightly out-competes the predictive skill by the Markov model (Fig. 8d).

Irrespective of these shortcomings, our results have demonstrated that even a zero-dimensional 1st order linear Markov model driven by observed precipitation variability could generate skillful forecasts by initializing the observed soil water. For such empirical forecasts regionally

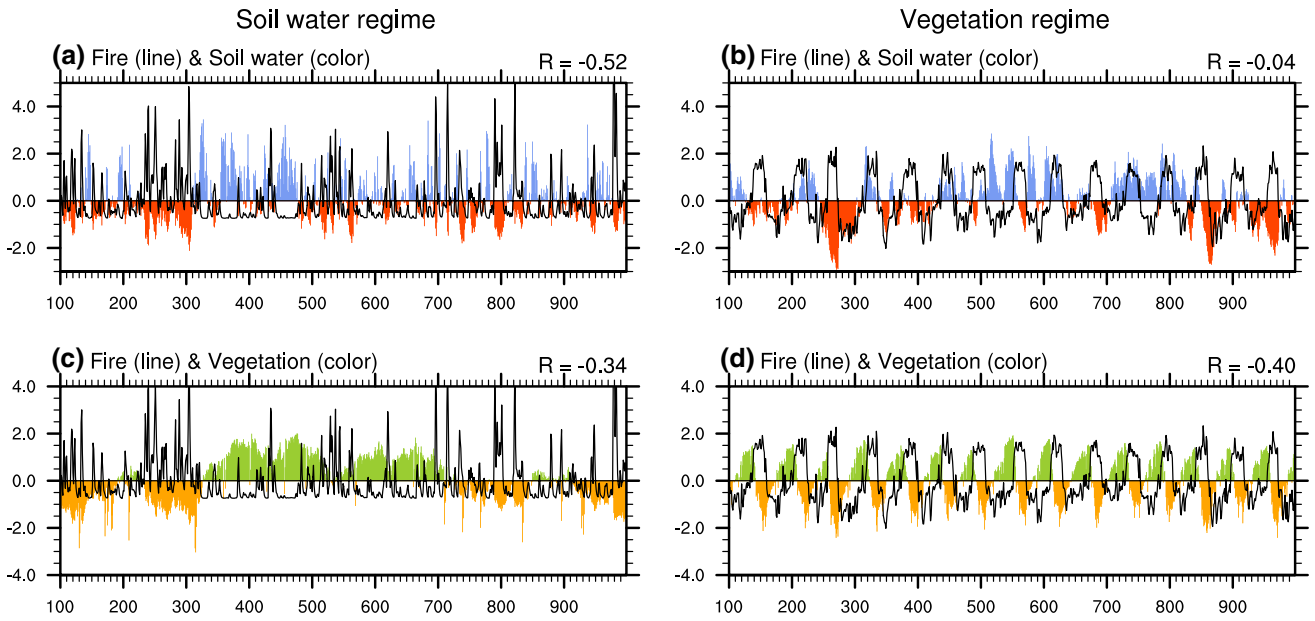

Fig. 16 Same as Fig. 10 but for the soil water and the vegetation regimes. The soil water and the vegetation regimes are obtained from the nearest grip points at (46N, 107.5W) and (35N, 117.5W) represented by S and V marks in Fig. 15, respectively

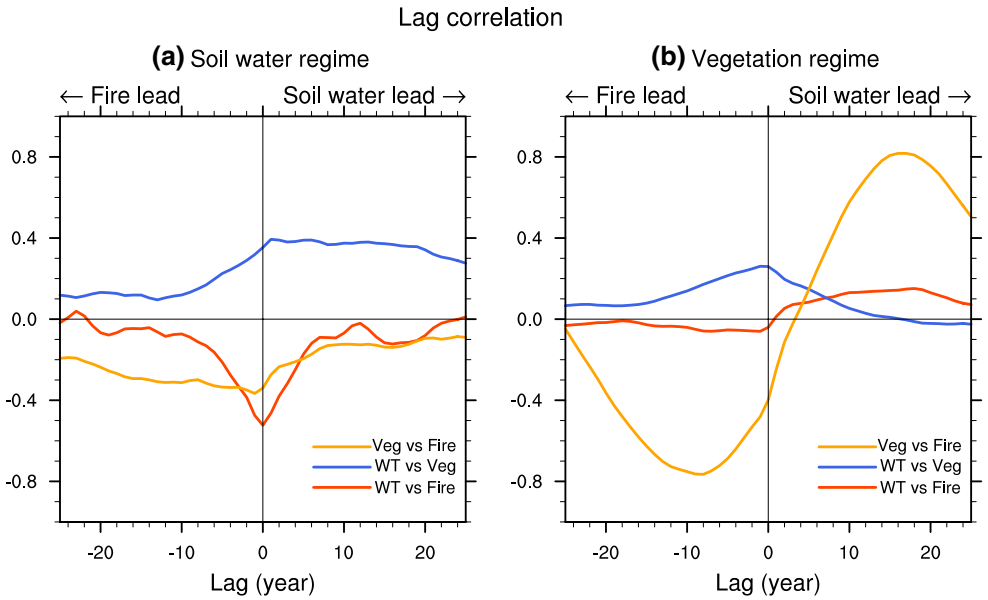

Fig. 17 Same as Fig. 11 but for the soil water and the vegetation regimes

depth-dependent damping rates $\lambda(x, y, z)$ could be derived from the lag-1 autocorrelation of long term observational records of water storage and soil moisture. Although water storage and soil moisture are difficult to observe with sufficient spatial coverage, observational reconstructions of land hydrological variables and fire cycles (Maurer et al. 2002; van den Dool et al. 2003; Fan and van den Dool 2004; Littell et al. 2009; Wada et al. 2010) may still provide useful information to determine potential longer-term predictabilities. Recent advances in observing water storage and drought from satellite sensors (Anderson et al. 2011; Famiglietti et al. 2011) could further help to improve the initialization of statistical and numerical forecasts of soil moisture on interannual to decadal timescales.

Unresolved issues that will be addressed in a series of forthcoming studies include the effects of ocean dynamics

on the predictability of low-frequency atmosphere and land variability and the feedback of soil moisture variations on atmospheric temperatures and circulation (e.g., Rowntree and Bolton 1983; Atlas et al. 1993; Koster et al. 2000).

6 Conclusions

We have evaluated the potential decadal predictability of variations in soil water, vegetation, and fire frequency over North America using the low resolution version of the earth system model CESM. Consistent with the previous studies, we find virtually no skill of annual mean precipitation beyond 1 or 2 years lead time. The dominant temporal variability of the leading EOF mode for annual precipitation can essentially be described as a white noise process. In contrast, the dominant mode of total water storage exhibits a large degree of redness, which translates into decadal predictability of depth integrated soil moisture, particularly for the deep soil layers.

Our study revealed that the stochastic climate model concept of a 1st order linear Markov process (Hasselmann 1976; Delworth and Manabe 1988) can be successfully applied to understand first order decadal variability and predictability of hydroclimate variations across North America. Soils act as an integrator and natural low-pass filter of white noise precipitation variability. Associated with the long-term predictability of soil water and internal slow vegetation adjustment timescales, we also found evidence for decadal predictability of total vegetation carbon and fire season length in the CESM experiments.

Finally, we studied whether potential decadal predictability of soil water would provide a means to ascertain wildfire risks across North America. The result strongly depends on the prevailing local fire regime. In dry areas, there is an increased chance to find the so-called vegetation regime, whereas the soil water regime can be found in wetter regions. On average, we found higher predictability for the vegetation regime, in which the slow timescales of vegetation regrowth determine the fuel availability and hence the fire season length. Although our results are based on an idealized modeling framework that captures only naturally occurring climate variations, they clearly suggest that decadal climate predictions for soil hydrological conditions are feasible and may become beneficial for forestry, water management, and agriculture.

Acknowledgments The manuscript benefited from the constructive comments of two anonymous reviewers. This work is supported through NSF Award No. 1049219, Investigation of Decadal Climate Predictability and Hydroclimate impacts (IDCPI) on the Western US. We thank the IDCPI group (N. Buenning, L. Kanner, D. Noone, L. Sloan, M. Snyder, L. Stott) for numerous stimulating discussions. M. Kimoto, R. Oishi, and A. Alessandri are acknowledged for their constructive comments. The CESM project is supported by the National Science Foundation and the Office of Science (BER) of the U.S. Department of Energy. Computation for the work described in this paper was supported by the University of Southern California Center for High-Performance Computing and Communications (hpcc.usc.edu). The GPCC, PREC/L, PDSI, and CPC datasets provided by the NOAA/OAR/ESRL PSD, Boulder, Colorado, USA, from their Web site at http://www.esrl.noaa.gov/psd/.

Open Access This article is distributed under the terms of the Creative Commons Attribution License which permits any use, distribution, and reproduction in any medium, provided the original author(s) and the source are credited.

References

Alessandri A, Borrelli A, Navarra A, Arribas A, Déqué M, Rogel P, Weisheimer A (2011) Evaluation of probabilistic quality and value of the ENSEMBLES multimodel seasonal forecasts: comparison with DEMETER. Mon Weather Rev 139(2):581–607

Amenu GG, Kumar P, Liang X-Z (2005) Interannual variability of deep-layer hydrologic memory and mechanisms of its influence on surface energy fluxes. J Clim 18(23):5024–5045

Anderson MC, Hain C, Wardlow B, Pimstein A, Mecikalski JR, Kustas WP (2011) Evaluation of drought indices based on thermal remote sensing of evapotranspiration over the continental United States. J Clim 24(8):2025–2044

Arora V, Boer G (2006) The temporal variability of soil moisture and surface hydrological quantities in a climate model. J Clim 19(22):5875–5888

Atlas R, Woldson N, Terry J (1993) The effect of SST and soil moisture anomalies on the GLA model simulation of the 1998 U.S. summer drought. J Clim 6:2034–2048

Barlow M, Nigam S, Berbery E (2001) ENSO, Pacific decadal variability, and US summertime precipitation, drought, and stream flow. J Clim 14(9):2105–2128

Beljaars A, Viterbo P, Miller M, Betts A (1996) The anomalous rainfall over the United States during July 1993: sensitivity to land surface paramterization and soil moisture anomalies. Mon Weather Rev 124:362–383

Bjerknes J (1964) Atlantic air–sea interaction. Adv Geophys 10(1):1–82

Bowman DM et al (2009) Fire in the earth system. Science 324(5926):481–484

Brown K, Clark J, Grimm E, Donovan J, Mueller P, Hansen B, Stefanova I (2005) Fire cycles in North American interior grasslands and their relation to prairie drought. Proc Natl Acad Sci USA 102(25):8865–8870

Chen J, Kumar P (2002) Role of terrestrial hydrologic memory in modulating ENSO impacts in North America. J Clim 15(24):3569–3585

Chen J, Kumar P (2004) A modeling study of the ENSO influence on the terrestrial energy profile in North America. J Clim 17(8):1657–1670

Chen M, Xie P, Janowiak JE, Arkin PA (2002) Global land precipitation: a 50-yr monthly analysis based on gauge observations. J Hydrometeorol 3(3):249–266

Chikamoto Y, Kimoto M, Watanabe M, Ishii M, Mochizuki T (2012) Relationship between the Pacific and Atlantic stepwise climate change during the 1990s. Geophys Res Lett 39(21):L21710

Chikamoto Y et al (2013) An overview of decadal climate predictability in a multi-model ensemble by climate model MIROC. Clim Dyn 40:1201–1222. doi:10.1007/s00382-012-1351-y

Coats S, Smerdon JE, Seager R, Cook BI, González-Rouco J (2013) Megadroughts in southwestern North America in

millennium-length ECHO-G simulations and their comparison to proxy drought reconstructions. J Clim 26(2013):7635–7649. doi:10.1175/JCLI-D-12-00603.1
Collins M (2002) Climate predictability on interannual to decadal time scales: the initial value problem. Clim Dyn 19(8):671–692
Cook B, Miller R, Seager R (2009) Amplification of the North American Dust Bowl drought through human-induced land degradation. Proc Natl Acad Sci USA 106(13):4997–5001
Dai A (2011) Drought under global warming: a review. Wiley Interdiscip Rev Clim Change 2(1):45–65
Dai A (2013) Increasing drought under global warming in observations and models. Nature Clim Change 3:52–58. doi:10.1038/nclimate1633
Delworth TL, Manabe S (1988) The influence of potential evaporation on the varibilities of simulated soil wetness and climate. J Clim 1:523–547
Dirmeyer PA, Kumar S, Fennessy MJ, Altshuler EL, DelSole T, Guo Z, Cash BA, Straus D (2013) Model estimates of land-driven predictability in a changing climate from CCSM4. J Clim 26(21):8495–8512
Famiglietti J et al (2011) Satellites measure recent rates of groundwater depletion in California's central valley. Geophys Res Lett 38(3):L03403
Fan Y, van den Dool H (2004) Climate prediction center global monthly soil moisture data set at 0.5 resolution for 1948 to present. J Geophys Res Atmos 109:D10102
Farris CA, Baisan CH, Falk DA, Yool SR, Swetnam TW (2010) Spatial and temporal corroboration of a fire-scar-based fire history in a frequently burned ponderosa pine forest. Ecol Appl 20(6):1598–1614
Gent P et al (2011) The community climate system model version 4. J Clim 24(19):4973–4991
Hasselmann K (1976) Stochastic climate models. Part I. Theory. Tellus 28:473–485
Hu A, Meehl GA, Han W, Yin J, Wu B, Kimoto M (2013) Influence of continental ice retreat on future global climate. J Clim 26:3087–3111
Jochum M, Fox-Kemper B, Molnar P, Shields C (2009) Differences in the indonesian seaway in a coupled climate model and their relevance to pliocene climate and El Niño. Paleoceanography 24:PA1212
Kanamitsu M, Lu C, Schemm J, Ebisuzaki W (2003) The predictability of soil moisture and near-surface temperature in hindcasts of the NCEP seasonal forecast model. J Clim 16(3):510–521
Katul GG, Porporato A, Siqueira M (2007) On the spectrum of soil moisture from hourly to interannual scales. Water Resourc Res 43:W05428. doi:10.1029/2006WR005356
Keenlyside NS, Latif M, Jungclaus J, Kornblueh L, Roeckner E (2008) Advancing decadal-scale climate prediction in the North Atlantic sector. Nature 453:84–88. doi:10.1038/nature06921
Kloster S et al (2010) Fire dynamics during the 20th century simulated by the community land model. Biogeosciences 7(6):1877–1902. doi:10.5194/bg-7-1877-2010
Koster R, Suarez M, Heiser M (2000) Variance and predictability of precipitation at seasonal-to-interannual timescales. J Hydrometeorol 1:26–46
Koster RD, Suarez MJ (2003) Impact of land surface initialization on seasonal precipitation and temperature prediction. J Hydrometeorol 4(2):408–423
Langford S, Stevenson S, Noone D (2014) Analysis of low-frequency precipitation variability in CMIP5 historical simulations for southwestern North America. J Clim 27(2014):2735–2756. doi:10.1175/JCLI-D-13-00317.1
Lawrence D, Oleson K, Flanner M, Fletcher C, Lawrence P, Levis S, Swenson S, Bonan G (2012) The CCSM4 land simulation, 1850–2005: assessment of surface climate and new capabilities. J Clim 25(7):2240–2260
Lehmann CE et al (2014) Savanna vegetation-fire-climate relationships differ among continents. Science 343(6170):548–552
Littell JS, McKenzie D, Peterson DL, Westerling AL (2009) Climate and wildfire area burned in western US ecoprovinces, 1916–2003. Ecol Appl 19(4):1003–1021
Maurer E, Wood A, Adam J, Lettenmaier D, Nijssen B (2002) A long-term hydrologically based dataset of land surface fluxes and states for the conterminous United States. J Clim 15(22):9384–9392
McCabe G, Betancourt J, Gray S, Palecki M, Hidalgo H (2008) Associations of multi-decadal sea-surface temperature variability with US drought. Quat Int 188(1):31–40
McCabe-Glynn S, Johnson KR, Strong C, Berkelhammer M, Sinha A, Cheng H, Edwards RL (2013) Variable North Pacific influence on drought in southwestern North America since ad 854. Nature Geosci 6:617–621
McGregor S, Timmermann A, Stuecker MF, England MH, Merrifield M, Jin F-F, Chikamoto Y (2014) Recent Walker circulation strengthening and Pacific cooling amplified by Atlantic warming. Nature Clim Change 4:888–892. doi:10.1038/nclimate2330
Meehl G, Hu A (2006) Megadroughts in the Indian monsoon region and southwest North America and a mechanism for associated multidecadal Pacific sea surface temperature anomalies. J Clim 19(9):1605–1623
Meehl GA et al (2014) Decadal climate prediction: an update from the trenches. Bull Am Meteorol Soc 95:243–267
Mochizuki T et al (2010) Pacific decadal oscillation hindcasts relevant to near-term climate prediction. Proc Natl Acad Sci USA 107:1833. doi:10.1073/pnas.0906531107
Murphy J et al (2010) Towards prediction of decadal climate variability and change. Procedia Environ Sci 1:287–304
Neale RB, Richter J, Park S, Lauritzen PH, Vavrus SJ, Rasch PJ, Zhang M (2013) The mean climate of the community atmosphere model (CAM4) in forced sst and fully coupled experiments. J Clim 26(14):5150–5168
Niu G, Yang Z (2007) An observation-based formulation of snow cover fraction and its evaluation over large North American river basins. J Geophys Res 112:D21101
Oleson K et al (2008) Improvements to the community land model and their impact on the hydrological cycle. J Geophys Res 113:G01021
Rowntree P, Bolton J (1983) Simulation of the atmospheric response to soil moisture anomalies over Europe. Quat J R Meteorol Soc 109:501–526
Schneider U, Becker A, Finger P, Meyer-Christoffer A, Rudolf B, Ziese M (2011) GPCC full data reanalysis version 6.0 at 1.0: monthly land-surface precipitation from rain-gauges built on GTS-based and historic data. doi:10.5676/DWD_GPCC/FD_M_V6_100
Schubert S, Koster R, Hoerling M, Seager R, Lettenmaier D, Kumar A, Gutzler D (2007) Predicting drought on seasonal-to-decadal time scales. Bull Am Meteorol Soc 88(10):1625
Schubert S, Suarez M, Pegion P, Koster R, Bacmeister J (2004) On the cause of the 1930s dust bowl. Science 303(5665):1855–1859
Schubert S et al (2009) A US CLIVAR project to assess and compare the responses of global climate models to drought-related SST forcing patterns: overview and results. J Clim 22(19):5251–5272
Seager R, Burgman R, Kushnir Y, Clement A, Cook E, Naik N, Miller J (2008) Tropical Pacific forcing of North American medieval megadroughts: testing the concept with an atmosphere model forced by coral-reconstructed SSTs. J Clim 21(23):6175–6190
Seager R, Kushnir Y, Herweijer C, Naik N, Velez J (2005) Modeling of tropical forcing of persistent droughts and pluvials over western North America: 1856–2000. J Clim 18(19):4065–4088
Seager R, Naik N, Ting M, Cane M, Harnik N, Kushnir Y (2010) Adjustment of the atmospheric circulation to tropical Pacific SST anomalies: variability of transient eddy propagation in

the Pacific-North America sector. Quart J R Meteorol Soc 136(647):277–296
Seneviratne SI, Corti T, Davin EL, Hirschi M, Jaeger EB, Lehner I, Orlowsky B, Teuling AJ (2010) Investigating soil moisture–climate interactions in a changing climate: a review. Earth Sci Rev 99(3):125–161
Sheffield J, Wood E (2008) Global trends and variability in soil moisture and drought characteristics, 1950–2000, from observation-driven simulations of the terrestrial hydrologic cycle. J Clim 21(3):432–458
Shields C, Bailey D, Danabasoglu G, Jochum M, Kiehl J, Levis S, Park S (2012) The low-resolution CCSM4. J Clim 25(12):3993–4014
Shin S-I, Sardeshmukh PD (2011) Critical influence of the pattern of tropical ocean warming on remote climate trends. Clim Dyn 36(7):1577–1591
Smith DM, Cusack S, Colman AW, Folland CK, Harris GR, Murphy JM (2007) Improved surface temperature prediction for the coming decade from a global climate model. Science 317:796–799. doi:10.1126/science.1139540
Smith TM, Reynolds RW, Peterson TC, Lawrimore J (2008) Improvements to NOAA's historical merged land-ocean surface temperature analysis (1880–2006). J Clim 21(10):2283–2296
Stahle DW, Fye FK, Cook ER, Griffin RD (2007) Tree-ring reconstructed megadroughts over North America since AD 1300. Clim Change 83(1–2):133–149
Stevenson S, Fox-Kemper B, Jochum M (2012) Understanding the ENSO-CO2 link using stabilized climate simulations. J Clim 25(22):7917–7936
Stevenson SL, Timermann A, Chikamoto Y, Langford S, DiNezio P (2014) Stochastically generated North American megadroughts. J Clim. doi:10.1175/JCLI-D-13-00689.1
Svoboda M et al (2002) The drought monitor. Bull Am Meteorol Soc 83:1181–1190
Swetnam TW, Betancourt JL (1998) Mesoscale disturbance and ecological response to decadal climatic variability in the American southwest. J Clim 11(12):3128–3147
Taylor K, Stouffer R, Meehl G (2009) A summary of the CMIP5 experiment design. http://cmip-pcmdi.llnl.gov/cmip5/docs/Taylor_CMIP5_design
Thonicke K, Venevsky S, Sitch S, Cramer W (2001) The role of fire disturbance for global vegetation dynamics: coupling fire into a dynamic global vegetation model. Global Ecol Biogeogr 10(6):661–677
Thornley J, Cannell M (2004) Long-term effects of fire frequency on carbon storage and productivity of boreal forests: a modeling study. Tree Physiol 24(7):765–773
van den Dool H, Huang J, Fan Y (2003) Performance and analysis of the constructed analogue method applied to US soil moisture over 1981–2001. J Geophys Res Atmos 108(D16):8617
van der Werf GR, Randerson JT, Collatz GJ, Giglio L, Kasibhatla PS, Arellano AF, Olsen SC, Kasischke ES (2004) Continental-scale partitioning of fire emissions during the 1997 to 2001 El Niño/La Niña period. Science 303(5654):73–76
van Oldenborgh GJ, Doblas-Reyes FJ, Wouters B, Hazeleger W (2012) Decadal prediction skill in a multi-model ensemble. Clim Dyn 38:1263–1280
Viegas D, Viegas M, Ferreira A (1992) Moisture content of fine forest fuels and fire occurrence in central Portugal. Int J Wildland Fire 2(2):69–86
Wada Y, van Beek L, van Kempen C, Reckman J, Vasak S, Bierkens M (2010) Global depletion of groundwater resources. Geophys Res Lett 37(20):L20402
Wang F, Liu Z, Notaro M (2013) Extracting the dominant SST modes impacting North America's observed climate. J Clim 26(15):5434–5452
Wang W, Kumar A (1998) A GCM assessment of atmospheric seasonal predictability associated with soil moisture anomalies over North America. J Geophys Res Atmos 103(D22):28637–28646
Westerling A, Gershunov A, Brown T, Cayan D, Dettinger M (2003) Climate and wildfire in the western United States. Bull Am Meteorol Soc 84(5):595–604
Woodhouse C, Overpeck J (1998) 2000 years of drought variability in the central United States. Bull Am Meteorol Soc 79(12):2693–2714
Wu W, Geller MA, Dickinson RE (2002) The response of soil moisture to long-term variability of precipitation. J Hydrometeorol 3(5):604–613
Yang F, Kumar A, Lau K (2004) Potential predictability of US summer climate with perfect soil moisture. J Hydrometeorol 5(5):883–895
Zeng N, Neelin J, Lau K, Tucker C (1999) Enhancement of interdecadal climate variability in the Sahel by vegetation interaction. Science 286(5444):1537–1540